IMPACT OF MANUFACTURING IMPERFECTIONS AND EXTREME THERMAL AND PHYSICAL STRESS ON THE PERFORMANCE OF ELECTROMECHANICAL ENERGY CONVERTERS

by

Seethal Jayasankar

APPROVED BY SUPERVISORY COMMITTEE:

Dr. Babak Fahimi, Chair

Dr. Poras T. Balsara

Dr. Mehrdad Nourani

Dr. Ann Catrina Coleman

This thesis is dedicated to my loving parents, Dr. Reeta Jayasankar and Dr. P. Jayasankar, without whose support and dedication none of my success would have been possible

IMPACT OF MANUFACTURING IMPERFECTIONS AND EXTREME THERMAL AND PHYSICAL STRESS ON THE PERFORMANCE OF ELECTROMECHANICAL ENERGY CONVERTERS

by

SEETHAL JAYASANKAR, BE

THESIS

Presented to the Faculty of

The University of Texas at Dallas

in Partial Fulfillment

of the Requirements

for the Degree of

MASTER OF SCIENCE IN

ELECTRICAL ENGINEERING

THE UNIVERSITY OF TEXAS AT DALLAS

August 2017

ACKNOWLEDGMENTS

I would like to express my sincere gratitude towards my advisor Dr. Babak Fahimi for giving me the wonderful opportunity to work at the Renewable Energy and Vehicular Technology Laboratory. Dr. Fahimi's constant support and guidance has been very beneficial and will certainly continue to help me in my future endeavors. I would like to thank my committee members, Dr. Poras T. Balsara, Dr. Mehrdad Nourani and Dr. Ann Catrina Coleman for taking time out from their busy schedules and providing me with their constructive comments and suggestions.

I would like to thank my family and friends for their unconditional support especially Utsav Vijay Dholakia, Misha Hemantkumar Mehta, Eva Cosoroaba, Jingchen Liang and Lizon Maharjan. My friends at the REVT laboratory have been very supportive throughout this journey and have helped me with their technical knowledge and guidance to achieve my goals. I would like to extend my deepest gratitude to all my friends at REVT.

Finally, I would like to thank my mother, Dr. Reeta Jayasankar, for all her sacrifices she has made to get me to the standings I am currently in.

June 2017

IMPACT OF MANUFACTURING IMPERFECTIONS AND EXTREME THERMAL

AND

PHYSICAL STRESS ON THE PERFORMANCE OF ELECTROMECHANICAL

ENERGY CONVERTERS

Seethal Jayasankar, MS
The University of Texas at Dallas, 2017

Supervising Professor: Dr. Babak Fahimi, Chair

This thesis discusses important factors that affect the performance of a machine. These are categorized based on the manufacturing processes of the magnetic steel and effects of high-energy magnets on the rotor core of specific machines.

The first factor examines the effects of cutting process such as Punch, Laser-jet and Water-jet on the magnetic properties of the core. The critical components such as relative permeability and core loss characteristics of the ferromagnetic core are discussed to study their effect on the overall performance of the machine.

The second factor as previously mentioned focuses on the influence of high-energy magnets on the magnetic properties of steel laminations in Permanent Magnet Synchronous Machines (PMSM). Relative permeability of the lamination is found to decrease when it is kept in contact with high-energy magnets for a prolonged period of time.

The significance of these two factors on the design of motors has been highlighted. Experiments and simulations are conducted to study the effects of these factors on the torque and speed characteristics of the machine.

TABLE OF CONTENTS

LIST OF FIGURES

LIST OF TABLES

CHAPTER 1

INTRODUCTION

1.1 Current Technology of Compact Motors

New motor technologies are trending towards higher efficiencies while keeping the size and weight of the motor to be small. Compact motors are used for wide variety of applications including automotive, medical, aerospace and domestic applications. The present demand in market is to come up with compact motors that produce higher power density, torque density and efficiency.

There are different factors that influence the efficiency of motors. It includes the Conductor Properties, Magnetic Steel, Thermal Design, Aerodynamic Design and Manufacturing Processes [2].

The Conductor Properties primarily deals with the resistive losses caused due to the conductor windings that account for 35% of the losses [2].

Magnetic steel is considered to be the most expensive component of the machine and the losses associated with it mainly include hysteresis and eddy current losses.

Thermal design emphasizes on cooling design techniques that reduce the clearance distance and lower the copper losses in the system. This helps the motor to run at a lower operating temperature and increases the service life of the motor.

Aerodynamic design is associated with the optimized design of the fan to produce more efficient cooling with a lower noise level.

Manufacturing Processes deals with the introduction of extreme thermal and physical stresses in the magnetic steel caused due to the different manufacturing processes such as cutting, riveting, welding and motor assembly which is found to increase the iron losses by up to 50% [2].

This thesis is mainly focused on the Magnetic Steel properties and the manufacturing processes of machine core that influences the efficiency of the machine. Efforts are made to showcase the effects of the different cutting techniques on the permeability and core losses of the machine. In addition to the manufacturing processes, experiments are performed to examine the influence of high energy magnets on the magnetic properties of the rotor core of Permanent Magnet Synchronous Machines (PMSM). It is concluded through a series of experiments that when magnetic steel is kept in contact with high energy magnets, it causes significant ageing effects on the magnetic steel core.

1.2 Effects of Manufacturing Processes

The deterioration of the magnetic properties of the non-oriented magnetic steel lamination caused by different manufacturing processes is a well-known issue. Efforts are needed to address this problem and choose manufacturing techniques which may be less detrimental to the overall efficiency of the machine. The manufacturing processes that cause the variation in performance may include cutting, welding, riveting, etc.

1.2.1 Residual Stress

Manufacturing processes are known to induce stress on the magnetic material. For detailed knowledge of how it may affect the machine, it is essential to know more about the stress present in the material. Stress in a magnetic material are mainly classified into two types [17]:

- Applied stress: Stress that is caused due to external forces.
- Residual stress: Stress that remains in the body after all the external forces are removed.

It is important to focus on the residual stress since it remains in the material even after removal of the external forces.

Residual stress are further divided into macro and micro stress. Macro stress are constant over long distances while the micro stress change in magnitude at distances much lesser than the normal grain diameter [17].

Macro stress is the main concern for the magnetic material since it causes fatigue and fracture and mainly occurs due to the plastic flow that appear during the manufacturing processes. This stress is overcome by post annealing methods. As discussed in Chapter 2, experiments conducted clearly shows that post annealing processes improves the magnetic properties of the magnetic material.

Microstress is mainly caused due to crystal imperfections and affects the domain wall movement in the material. It cannot be removed completely even after annealing.

1.2.2 Effects of Surface Abrasion on the Magnetic Properties of Silicon Steel

The different manufacturing processes of steel causes surface abrasion which in turn produces anisotropic strains in the steel samples. The effects can be explained by the domain theory of ferromagnetism which states that a sufficiently higher tension in materials having a positive magnetostriction can cause the domains to be oriented in parallel to the direction of applied tension.

Magnetostriction is defined as the property of ferromagnetic material that causes it to change shape or dimension when magnetized. It was first observed by Joule [28] who noted that the amount of elongation occuring in an iron wire was reduced if the wire was under tension. Magnetostriction occurs due to spin-orbit coupling.

A crystal of iron under no external strain, will have six possible directions of stable domain orientation (paramagnetic state when material is above curie temperature). The domains are magnetized to saturation [11].

When a field is applied in the easily magnetized direction of cube i.e [100], an increase in volume of the magnetized domains is observed parallel to the direction of the applied field in addition to a decrease in volume of domains in the reverse and lateral directions. The iron then changes shape from a cubic structure to a tetragonal structure with a longer axis at the [100] direction.

According to Ewing's theory, the atoms present in a ferromagnetic material are permanent magnets whose mutual interaction leads to the magnetic properties of the material. This theory was then superseded by the modern domain theory which states that the atoms are considered to have a magnetic moment due to "uncompensated spins" of electrons in the outer shell of the atomic structure.

Therefore, it can be said that surface abrasion can cause defects in the crystal structure of the material thus affecting its magnetic properties. According to [36], it was observed that when a cold rolled silicon sheet sample with a thickness of .012 inches, underwent surface abrasion of 100 micron-inches, there were still large changes in the magnetostriction and permeability and the effects were dependent on the direction of abrasion. The author also observed similar properties for hot-rolled silicon transformer sheet.

The observations were made under conditions of longitudinal, transverse and 45° angle abrasions. A transverse abrasion was found to produce longitudinal tension and therefore had reduction in magnetostriction and increase in permeability. On the other hand, the longitudinal abrasion produced transverse tension which means the tension was at right angles to the direction of field. Therefore majority of the domains were directed at right angles to the field which caused an increase in magnetostriction and a decrease in permeability.

Figure 1.1 [36] shows the magnetostriction for the samples of cold rolled silicon steel with abrasion in longitudinal, transverse and 45° angle. It can be clearly observed that effects of magnetostriction is completely dependent on the direction of abrasion.

The permeability of the samples were also noted in order to understand the effects of abrasion on the magnetic steel samples. It was observed that the large increase in magnetostriction was accompanied by a reduction of permeability. Figure 1.2 [36] shows the change in permeability with respect to flux densities at different directions of abrasion.

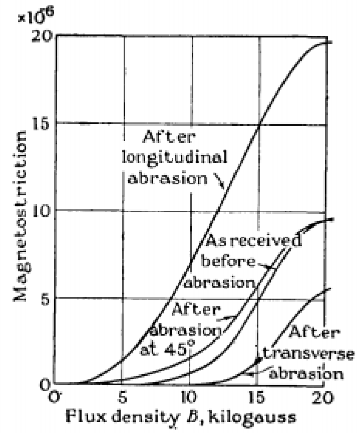

Figure 1.1. Change in magnetostriction for samples of cold-rolled silicon steel with abrasions in different directions (Source: R. G. Martindale, "Anisotropic strains produced by surface abrasion, and their effect on the magnetic properties of silicon sheet steel," in Electrical Engineers - Part II: Power Engineering, Journal of the Institution of, vol. 95, no. 47, pp. 620-626, October 1948)

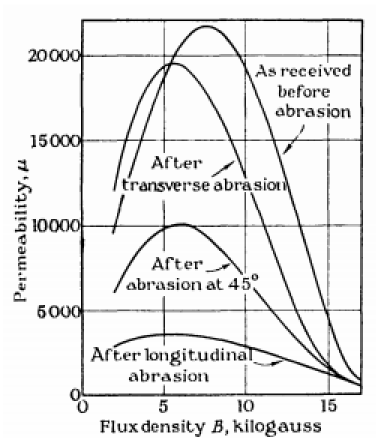

Figure 1.2. Change in permeability with respect to flux density for samples of cold-rolled silicon steel with abrasions in different directions (Source: R. G. Martindale, "Anisotropic strains produced by surface abrasion, and their effect on the magnetic properties of silicon sheet steel," in Electrical Engineers - Part II: Power Engineering, Journal of the Institution of, vol. 95, no. 47, pp. 620-626, October 1948)

Therefore, it was clear that the change in magnetostriction and permeability was dependent on the direction of abrasion.

Surface abrasion on one side of the steel layer forced a state of compression both in the direction of abrasion and at right angle to it, the latter stress being much higher whereas abrasion in both sides of the steel sheet caused the central layer to be in a state of tensile stress [36].

Manufacturing processes also cause tensile and compression stress in materials. Tensile stress is considered to be positive and compression stress negative (by convention). Through experiments conducted in [41], it was shown that tensile stress increased the slope of the initial and remanent magnetization curve whereas compressive stress caused a decrease in the slope of the curve.

Figure 1.3 and Figure 1.4 [41]shows a direct comparison of the above mentioned phenomenon. A tensile force of 100MPa is applied in the first case and a compressive force of -200MPa is applied in the second case.

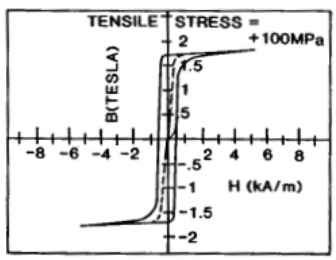

Figure 1.3. B-H curve at a tensile stress of +100MPa (Source: K. C. Pitman, "The influence of stress on ferromagnetic hysteresis," in IEEE Transactions on Magnetics, vol. 26, no. 5, pp. 1978-1980, Sep 1990)

1.2.3 Types of Cutting

The research in this thesis mainly focuses on the effects of two of the manufacturing processes, cutting and annealing, on the properties of magnetic steel. The commonly adopted cutting techniques are mechanical punching, laser cutting and waterjet cutting. These methods cause either mechanical or thermal stress that deteriorates the permeability and increases the core loss in the laminated steel.

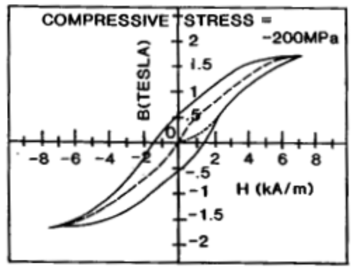

Figure 1.4. B-H curve at a compressive stress of -200MPa (Source: K. C. Pitman, "The influence of stress on ferromagnetic hysteresis," in IEEE Transactions on Magnetics, vol. 26, no. 5, pp. 1978-1980, Sep 1990)

This may affect crucial applications of motors in biomedical and aerospace industries where even a minor increase in the core loss can affect the efficiency of the motor thereby drastically affecting its performance.

The performance of samples produced through mechanical punching, laser cutting and waterjet cutting are studied through different experiments and are explained in detail in Chapter 2.

Mechanical Punching

Mechanical punching is the method that uses punch press to force a tool through the work-piece to form the desired material. The punch tool and the die are used for this process, and they are usually made of hardened steel or tungsten carbide.

Hammering or punching of steel sheets under high pressure causes surface compression. Since the sheet is subjected to such a treatment only on one side, it would curve the surface convex. When the load is removed, the boundaries of the sheet will not reverse back to the original position and the compression on the surface is retained.

Usually, punching is the most cost effective method for cutting and the processing speed is also quick. However, the precision is not as good as the other methods used [51] [33].

Laser-jet Cutting

Laser-jet cutting is a method that uses small laser beams to cut the materials. The laser is focused to produce a high-energy laser beam that can heat a small zone of the material to a very high temperature. The material in this zone is vaporized or melted.

There are several laser cutting methods applicable to different materials, such as vaporization cutting, melt and blow and thermal stress cracking, etc. Laser cutting is non-contact cutting, and has better precision and faster cutting speed but can cause heat-affected zones and thus cause thermal stress to the material [25].

Thermal stress or increase in temperature during the manufacturing process can affect the atomic structure of the material. In 1907 Weiss stated the idea of "molecular field" and "saturated domains" in ferromagnetic materials. It was explained that the magnetization of ferromagnetic materials occurred in discrete jumps. Heisenberg, Bethe and others concluded this theory using quantum mechanics.

It was explained that, at low temperature, when an element existed in its normal crystalline form and when the ratio of distance between the adjacent atoms to the diameter of the incomplete shell containing spinning electrons which caused the magnetic moment of the atom lay in the range of prescribed limits, then the spins were observed to be in the same direction with the spin axis parallel, thus spontaneously saturating the material.

However, when the temperature was increased, the alignment of the axis was disturbed and therefore the saturation fell to a lower value. The material was known to revert to the paramagnetic state at curie temperature.

Figure 1.5 [19] shows the variation of saturation magnetization with the increase in temperature for metals such as iron, cobalt and nickel. It can be clearly observed that with the rise in temperature, the saturation magnetization was found to decrease.

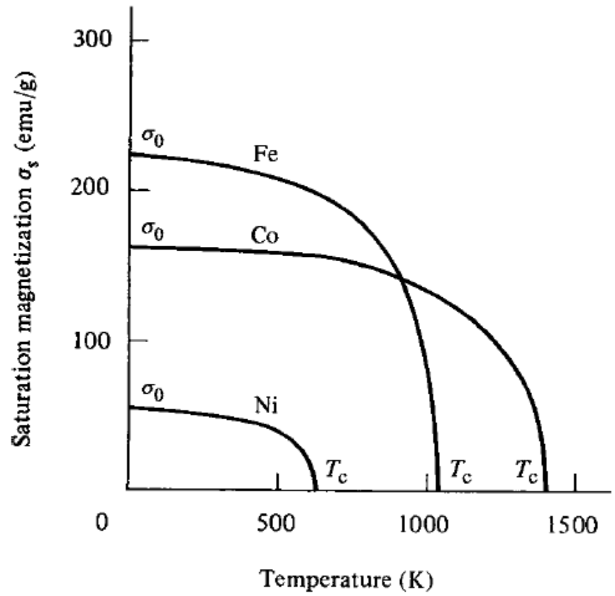

Figure 1.5. Change in saturation magnetization as a function of temperature (Source: Cullity, B. D. and C. D. Graham (2009d). Ferromagnetism, pp. 115-149. Wiley-IEEE Press.)

It can therefore be stated that the increase in temperature during the laser-cutting process can hamper the permeability and increase the core loss of the material as observed in experiments conducted (Chapter 2).

Water-jet Cutting

Water jet cutting is a method that is widely used in the industry. Basically, a water jet cutter uses high pressure water to cut materials. Depending on the application, the pressure varies from 1 mega Pascal to 100 mega Pascal. For soft materials, such as rubber and wood, a water jet cutter uses pure water as the cutting tool whereas for hard materials, such as stone and metal, the cutter uses mixture of water and abrasive substance (e.g. garnet) as the cutting tool.

The most important advantage of water jet cutting is that there is no heat-affected zone. Hence, the materials to be cut will stay at low temperature to prevent changing its heat-sensitive intrinsic properties [24].

1.2.4 Annealing

In addition to the cutting techniques, post-annealing processes also has an influence on the magnetic properties of the steel core. Annealing is a heat treatment process that alters the physical and chemical properties of a material in order to increase its ductility and reduce the hardness. It helps in recovery, recrystallization and grain growth in magnetic materials. The materials become magnetically softer after the annealing process.

According to [12], impurities present in the magnetic material can cause a decrease in its magnetic properties. An exhaustive study by Yensen [52] showed the effects of impurities such as carbon and sulphur on the magnetic properties of iron and silicon-iron. Figure 1.6 [52]shows the change in hysteresis losses due to impurities in iron at a maximum flux density of 10000 gauss.

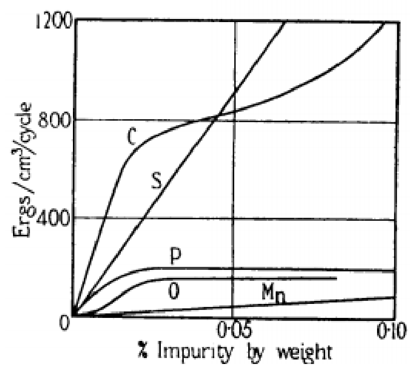

Figure 1.6. Change in hysteresis loss due to presence of impurities in iron (Source: Yensen, T. D. (1924, Jan). The magnetic properties of the ternary alloys fe-si-c. Transactions of the American Institute of Electrical Engineers XLIII, 145-175)

It can be observed that even small percentage of carbon and sulphur can be harmful. Annealing helps in removing such impurities and remarkably improves the magnetic properties of the sample.

In some experiments [12] annealing was performed in a hydrogen atmosphere at a high temperature. The initial and maximum permeability was observed to improve after the annealing process.

Magnetic annealing has also been found to improve the directional magnetic properties of magnetic steel [12]. It increases the permeability in a preferred direction and decreases the value in opposite and lateral directions. This is done by applying a magnetic field during the cooling process at the curie temperature.

In the experiments explained in Chapter 2, annealing of laminations was conducted after the cutting process. It was found to have a positive influence on the magnetic properties of the laminations. It was observed that the post-annealing processes improved the relative permeability of the core material, decreased the core-loss and also improved the surface finish of the laminations.

1.2.5 Surface Imperfections due to cutting

In addition to the magnetic properties of the steel samples, it is observed that the different cutting techniques have divergent effects on the surface of the sample particularly the edges.

In this thesis, the surface of different samples of steel cut by punching, laser-jet and water-jet cutting techniques are studied with the help of a digital microscope. It is observed through 3-D imaging that the Laser-jet sample is found to have the largest imperfections in comparison to the punch and water-jet samples. It is also observed that post-annealing process of the sample improves the surface finish and therefore reduces the core losses of the machine.

This is a very important factor that needs to be considered while designing a machine since the surface imperfections directly affect the air-gap of the machine. Larger air-gap causes higher losses and reduces the power density of the machine.

1.2.6 Literature Review

Several papers have been published which emphasizes the importance of the cutting and annealing techniques and its influence on the magnetic properties of the steel core.

It is well-known that the punch-cutting technique causes plastic deformation at the edges of the lamination and laser-cutting technique causes thermal-stress. In [22], Emura discusses the influence of different cutting techniques (punching, guillotine, laser and photo corrosion) before and after annealing at 1.5T. It is concluded that annealing before cutting does not improve the efficiency but annealing after cutting the steel can improve the efficiency of the steel core.

In [34], Lazari studies the influence of the laser cut on the performance of a Permanent Magnet Assisted Synchronous Reluctance Machine especially those showing an excessive cutting length per steel area. In [47], experiment shows the deterioration of the magnetic property in magnetic steel with the laser cutting and mechanical punching. [7] talks about the prediction of mechanical stress effects on the iron loss in electrical machines.

In [43], Rygal discusses about the influence of cutting stress on magnetic field and flux density distribution in non-oriented electrical steels. The impact would be more profound for small width of the strips such as stator teeth of electric machines. However, not much work has been done to investigate the influence of waterjet cutting on the B-H characteristics of electrical steel laminations.

In this study, experiments were performed to study the influence of the punch, laser-jet and water-jet cutting technique on the magnetic properties of the non-oriented magnetic steel. The experiments show that the water-jet cutting technique has the least influence on the magnetic properties of the ferromagnetic core. Punched and laser-cut laminations have higher core loss. Experiments and simulations show that post-annealing process conducted on the laser-jet cut sample improves the magnetic properties of the lamination.

1.3 Effects of ferromagnetic hysteresis loops on Inductive circuit

For the optimal design of electric motors, knowledge of core properties is of utmost importance. There are different factors that cause power losses in the ferromagnetic material. These have been studied continuously since the first formulation of power loss [50].

The magnetic losses are decomposed into hysteresis loss, $\mathrm{P_h}$ which is directly proportional to the frequency, eddy-current loss, $\mathrm{P_e}$ which directly depends on the square of the frequency [14] [26] and anomalous eddy current losses, $\mathrm{P_{anomalous}}$ caused by magnetic domain wall movement [8] [9].

$$P_v = P_h + P_e + P_{anomalous} \tag{1.1}$$

$\mathrm{P_v}$ is the total magnetic loss per unit volume. When iron loss separation techniques was investigated [10], it was observed that the hysteresis loss were more likely to be influenced by the deterioration caused due to the different manufacturing processes.

It was observed that the hysteresis loop of a laser-jet unannealed cut sample had the highest coercivity and least retentivity in comparison to water-jet cut sample. Therefore, it was important to study the characteristics of the hysteresis loop of the core and mathematically model the soft ferromagnetic core to study its influence on the performance of a machine.

Different models have been introduced in the past to study the non-linear hysteresis behavior of ferromagnetic materials. One such model is the Preisach model which was proved to accurately represent the hysteresis characteristics. But the implementation of the model was highly complex and required considerable computational time [53]. The other dynamic model that was widely accepted and easier to implement was the Jiles-Atherton model. It described, from a physical point of view, the hysteresis phenomenon that took place inside the soft ferromagnetic materials [27].

The parameters that are used in this model have physical significances and can be modified and obtained based on the manufacturing processes, materials used or change in the

B-H curve. It is a simple first order differential equation that calculates the magnetization of the sample with respect to the magnetic field based on these physical parameters.

Modified Jiles-Atherton equations were used to model the non-linear dynamic magnetic losses in the laminated steel of machines and to study the influence of the ferromagnetic hysteresis loop on the machine performance.

Different methods have been used to calculate the physical parameters of this model. One such method is the non-linear least square method which is based on curve fitting technique [29]. This method has been used in this thesis to calculate the Jiles-Atherton parameters.

A simple non-linear RL circuit was designed that displayed all the usual non-linear behavior. The influence of non-linear hysteresis was studied by comparing the exciting current waveforms of the RL circuit under conditions of linearity, saturation and non-linear hysteresis.

It was observed that under conditions of non-linear hysteresis, the current waveform was no longer perfectly triangular. The experiment was important to conclude the importance of the effects of B-H curves on the current waveforms which in turn affected the performance of the machine.

1.4 Influence of high-energy magnets on Magnetic Steel

In addition to the effects of different manufacturing processes, this thesis also focuses on the influence of high-energy magnets on the magnetic properties of the steel core.

Through experiments and simulations, it was observed that prolonged contact of the ferromagnetic core with high-energy magnets caused the relative permeability of the core sample to decrease substantially.

This is of paramount importance in machines such as Interior Permanent Magnet Synchronous Machines (IPMSM) and Surface Mount Permanent Magnet Synchronous Machines (SPMSM) where the rotor core is in continuous contact with high energy magnets.

1.4.1 High-energy rare earth magnets

For most applications, permanent magnet is used to produce a magnetic field because the field is formed without the use of any additional electric power or the production of heat that may cause losses [20]. For a material to be used as a permanent magnet, it needs to have an uniaxial anisotropy, a curie temperature above the room temperature and a high saturation magnetization. In addition, it is preferred to be inexpensive, have lower density and a good resistance against corrosion [20].

To attain higher power density and torque density ratings in motors, high-energy rare earth magnets are being used in machines. A magnetic field of a particular value can be produced by the geometrical configurations of these permanent magnets. Their large maximum energy product, $(BH)_{\mathrm{max}}$ helps to improve the performance of the machine.

Maximum energy product is the measure of magnetic energy which can be stored by a magnetic material. The energy is measured per unit volume of the magnetic material. According to [5] and [4] the samarium cobalt magnets have a maximum energy product of 33 MGOe and neodymium-iron-boron magnets can have maximum energy products of 52 MGOe.

Figure 1.7 [20] shows the comparison of maximum energy product of NdFeB in comparison to other magnetic materials.

For the experiments conducted in this thesis, Neodymium-iron-boron (NdFeB) were used.

They are known to have a curie temperature of 300^{o}C [20]. Although the performance benefits are undeniable but the use of rare earth magnets especially NdFeB has raised serious concerns in number of areas.

One of the major concerns is the cost fluctuation of these materials. It is also known to be susceptible to severe corrosion when used in moist conditions. But in addition to the mentioned reasons, it has also been found through this research that high-energy magnets affects the magnetic properties of the steel core.

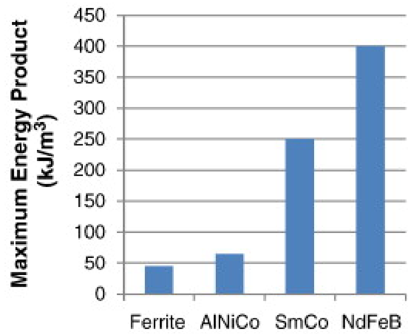

Figure 1.7. Comparison of maximum energy product of magnetic materials (Source: Cullity, B. D. and C. D. Graham (2009e). Hard Magnetic Materials, pp. 477-504. Wiley-IEEE Press.)

It was found that when high energy magnets were kept in contact with the magnetic steel for a period of four weeks, the permeability of the core decreased. It clearly showed that high-energy magnets could cause potential ageing effects of the steel core. The study also showed that these ageing effects had different influences on the motor at varied operating points.

These have to be known in detail and taken into consideration while designing the motors for different applications. It could therefore be concluded that it was very important to consider these factors while designing the core of PM motors since the decrease in relative permeability could lead to an increase in reluctance of the magnetic circuit which in turn could affect the inductance and flux density, hence altering the performance of the machine at a particular operating condition.

In the experiments conducted, three different criteria were considered in order to study the influence of high-energy magnets on the relative permeability of magnetic steel:

- The high-energy magnets were kept in contact with the magnetic steel for a period of four weeks. Data was collected every week and the change in permeability was noted.

- After keeping the magnet in contact with the magnetic steel for three weeks, the polarities of the magnets were reversed and the data was collected every week. Observations were made on the effects of polarity change.

- After keeping the magnet in contact with the magnetic steel for four weeks, the high-energy magnets were separated from the magnetic steel for the fifth week. Data was collected and readings were noted. The purpose of the experiment was to note if the magnetic steel regained its permeability after the separation of high-energy magnets.

Details of the experiment and results are discussed in Chapter 5 of the thesis.

1.5 Thesis Outline

The above sections mentioned a brief discussion about the contents of the thesis. The different chapters of this thesis is outlined below:

- Chapter 1: In this chapter, the new technology of compact motors is discussed. The problem statement is introduced and the content of the thesis is discussed.

- Chapter 2: This chapter discusses the effects of processing and cutting methods on the permeability, core loss and B-H curves of the steel core. Experiments are performed on the Punch, Laser-jet and Water-jet samples and results are discussed. Experiments are also performed to show the effects of post-annealing processes on the magnetic properties of the steel core.

- Chapter 3: In this section of the thesis, Effects of the hysteresis loop in an Inductive circuit is investigated. Non-linear Jiles-Atherton hysteresis model is simulated using MATLAB and excitation current waveforms are compared under different conditions of linearity, saturation and non-linear hysteresis.

- Chapter 4: This section of the thesis explains in detail the surface imperfections caused due to the different cutting methods. The effects of the surface imperfections on the machine performance such as air-gap length irregularities are explored and its influence on the power density and torque density are examined.

- Chapter 5: In this chapter, the influence of high-energy magnets on the performance of IPMSM and SPMSM machines are studied. Results of prolonged experiments conducted to explore the ageing effect of steel core due to high energy permanent magnets are discussed. ANSYS MAXWELL simulations are performed to show the effects of decrease in permeability on the inductance and rotor torque of an IPMSM machine.

- Chapter 6: Finally, this chapter summarizes the thesis, discusses the results of the experiments and simulations and outlines directions for future research.

CHAPTER 2

EFFECTS OF PROCESSING AND CUTTING METHODS ON THE MAGNETIC PROPERTIES OF FERROMAGNETIC CORE

In the first chapter of the thesis, a brief description of the problem statement and solution was discussed. It included the two main factors that was needed to be considered while designing motors, that is, the manufacturing processes of the laminations and the effects of high-energy magnets on the motor performance.

This chapter will focus on details about the ferromagnetic steel used in motor core, effects of different cuting techniques on the magnetic properties of these cores and in-depth comparisons with respect to crucial factors such as relative permeability and core loss.

2.1 Ferromagnetic Steel

The properties of a machine depends crucially on the geometry of the stator and rotor core, the air-gap between the stator and the rotor, properties of the core material such as hysteresis and permeability, the operating temperature of the core and the width of the laminations used to reduce the eddy currents. Ferromagnetic materials are used as cores in machines due to their high magnetic permeability. In the experiments that follow, a soft ferromagnet is used, which requires very less current to get magnetized.

Ferromagnetic materials consist of domains where the magnetic dipoles are parallel to each other [48]. When a field is applied to the ferromagnetic core, it gets magnetized.

The theory which was explained by Weiss discussed that the domains of the ferromagnet were spontaneously magnetized to a saturation value, but the direction of magnetization were in such a way that the net magnetization added to zero. The domains were separated by domains walls or a boundary. When a field was applied, the whole specimen shifted from a multi domain system to a single domain system by pushing the domain walls right out of the considered region, thus magnetizing the specimen in the direction of the applied field [19].

In most applications, it is undesirable for the core to retain the magnetization when the field is removed. This property of the core is known as ‘hysteresis’ and can cause energy loss. Therefore, ferromagnetic materials with lower hysteresis are preferred for the machine cores and are known as soft magnetic materials. But through experimental results conducted in this thesis, it is evaluated that the hysteresis losses of the core also depends on the cutting techniques used for manufacturing the steel core.

2.2 Core Loss

The core loss is created by varying the magnetic field in the core of the machine. The three main components of core loss is hysteresis loss, eddy-current loss and anomalous eddy current loss. All these components cause heating of the core and therefore reduces the efficiency of the machine.

2.2.1 Hysteresis Loss

Hysteresis loss depends on the microstructure of the ferromagnetic material [13]. The ferromagnetic material consists of uniformly magnetized structures that are known as domains.

Hysteresis in ferromagnetic materials is caused due to rotation of magnetization and change in size or number of these magnetic domains. When no magnetic field is provided, the sum of the magnetization is zero [30]. When a lower magnetic field is applied, the domain walls do not overcome the pinning sites formed due to the impurities found in the core [6] [30]. The impurities may include carbon, sulphur etc. At this point, if the field is removed, the magnetization of the material returns to zero. The slope of the curve in this region is known as the initial susceptibility [15].

But if a higher field is applied to the material, the magnetization becomes irreversible. Figure 2.1 [15] shows a sample B-H curve of a ferromagnetic material.

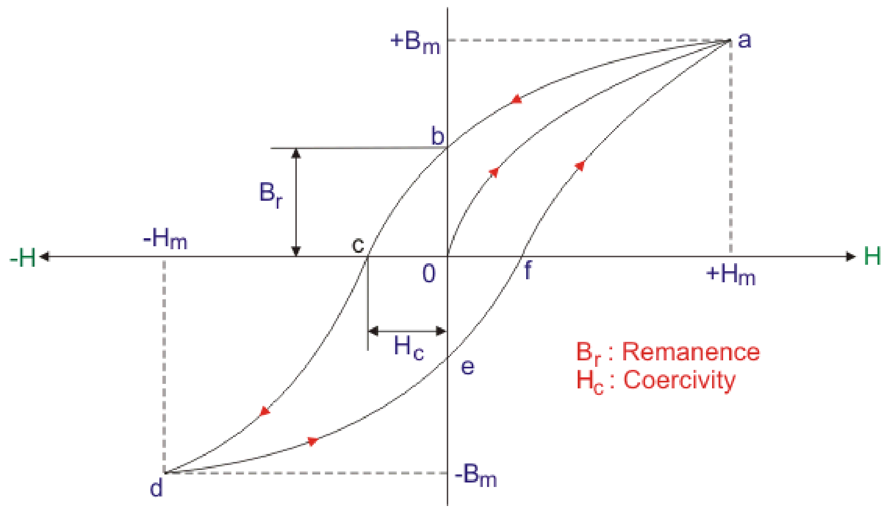

Figure 2.1. Initial susceptibility and B-H curve of Ferromagnetic Material (Source: Chikazumi, S. and C. D. Graham (2009). Physics of Ferromagnetism 2e. Number 94.Oxford University Press on Demand)

H_c is the coercivity of the ferromagnetic material which is defined as the ability of the material to withstand the external magnetic field without becoming demagnetized [1] and B_r is the retentivity or remanence which is defined as the residual magnetism left behind in the material after the external magnetic field is removed.

Another important factor to understand the nature of the material is its permeability. The ratio of magnetic flux density to the magnetic field applied is known as the permeability of the material. Permeability is an important qualitative measure for soft ferromagnetic materials due to below reasons [16]:

- Permeability varies with the magnetic field applied to the sample
- It is structure sensitive which means that it depends on factors such as heat treatment, deformation, purity etc.

These are crucial factors which gives an idea about the hysteresis loss of a ferromagnetic core.

2.2.2 Eddy Current Loss

Eddy current loss is caused due to closed loops of current induced in the ferromagnetic material due to the changing magnetic field. According to Lenz law, eddy current opposes the magnetic field that produces them [46]. Eddy current loss is harmful because they decrease the flux and produce heat which is proportional to i^2R where i is the eddy current and R is the resistance of the magnetic path.

These losses can be reduced by dividing the magnetic core into thin sheets of laminations. When the lamination sheets are electrically insulated to each other, the current is forced to circulate with their own lamination. This reduces the resistance of the magnetic path and the area of cross-section. The induced emf is also reduced and the net eddy current loss decreases.

2.2.3 Mathematical Model

Different mathematical models have been defined in literature to explain the core loss and to separate the hysteresis and eddy current loss. Details of the models can be found in [31].

Steinmetz equation and Bertotti's model was used in this thesis in order to study the effects of different cutting techniques on the hysteresis loss of the magnetic core.

According to the Steinmetz power law equation [50] [42]:

$$P_v(t) = K_h F^{\alpha} B_{max}^{\beta} \tag{2.1}$$

$P_{\mathrm{v}}(t)$ is the core loss in $\mathrm{mW/cm^3}$, K_{h} is the hysteresis constant, F is the frequency in Hz, B_{max} is the maximum flux density in Tesla and α and β are the curve fitting coefficients.

The total core loss was separated into hysteresis and eddy current loss using the Bertottis model at a lower frequency of 50Hz where the hysteresis loss was dominant over the eddy current loss.

According to the Bertotti's model [9]:

$$P_v(t) = K_h F B_{max}^{\beta} + K_c \sigma F^2 B_{max}^2 + 8\sqrt{\sigma G S V_o} F^{1.5} B_{max}^{1.5} \tag{2.2}$$

σ is the conductivity of the material, S is the cross-sectional area of the magnetic core, G is a constant with value 0.1356 and V_o is curve-fitting coefficient. K_c is the eddy current loss constant and depends on the geometry of the material.

The first term of the equation stands for the hysteresis loss, the second term is the classical eddy current loss and the third term stands for the extra eddy current loss/anomalous loss.

Bertotti's model was used for the calculation since it took into account the eddy current loss that occurred due to the domain wall movement.

2.3 Experimental Setup

In the experiments conducted, four samples of M-19 cores made with different cutting techniques were used [32].

The first sample was cut using the punch process, the second sample was cut using laser-jet cutting technique and the third sample was cut using the water-jet cutting technique. In order to compare the influence of post-annealing process on the magnetic properties of the ferromagnetic material, a fourth sample of annealed laser-jet cutting technique was used in the experiment.

Each sample consisted of two E-cores which were combined together to form a magnetic path. All four cores consisted of 28 pieces of 29 gauge M-19 steel laminations.

The E-cores were formed by welding the stack of lamination. Two coils were wound around with 300 turns at the center leg of each E-core sample to create primary and secondary windings for the B-H analyzer. The magnetic center path length was 228.6 mm and the cross-sectional area of the middle leg was 124.46 mm^2 for each sample.

Figure 2.2 shows the test object and winding arrangement used for the experiment.

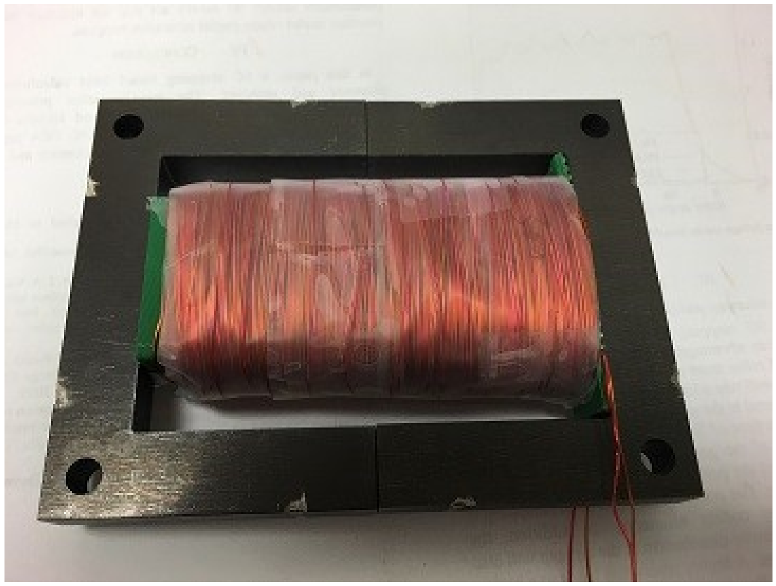

Figure 2.2. Illustration of the E-core

Figure 2.3 shows the experimental setup used to determine the relative permeability, core loss, and B-H curves for the different samples.

It comprised of a Hi-speed bipolar amplifier HSA 4014-IW and an IWATSU SY-955 B-H analyzer. The gain of the power amplifier was set to 10 [32].

2.4 Experimental Process

The different E-core samples were tested using the B-H analyzer.

B-H analyzer implements the two coil method to calculate the magnetic field strength H and a magnetic flux density B. Figure 2.4 represents the circuit configuration used by B-H analyzer to make the measurements.

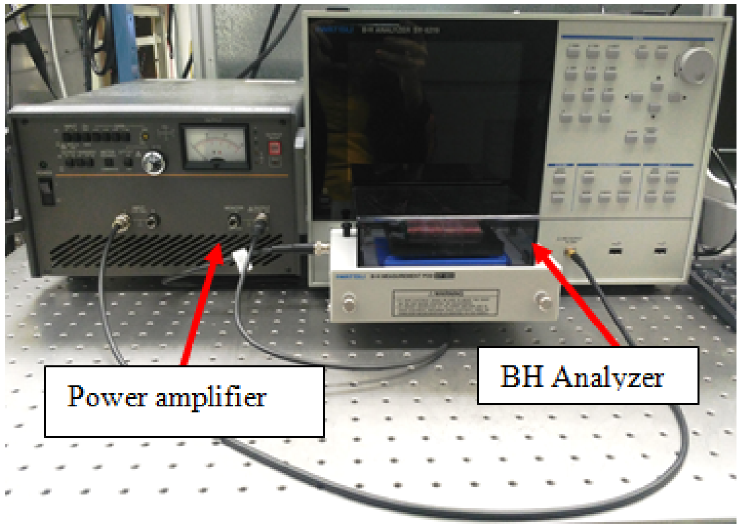

Figure 2.3. Experimental Setup

Primary turns were wound on the sample for providing excitation and the secondary turns were used for detecting the magnetic flux density. Pulse input was provided in all four cases.

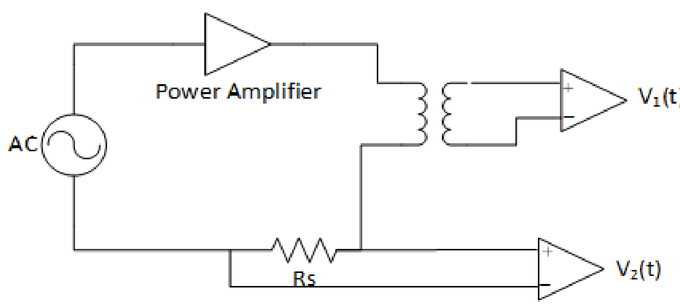

Figure 2.4. Diagram outlining the measured sample

The power amplifier which was used along with the analyzer, helped amplify this signal allowing the current to flow through the primary windings. The shunt resistor R_s was used for output voltage $V_2(t)$ measurement. The magnetic field strength and flux density was calculated using the following equations:

$$H(t) = \frac{N_1 V_2(t)}{L_e R_s} \tag{2.3}$$

$$B(t) = \frac{1}{N_2 A_e} \int_0^t V(\tau) d\tau \tag{2.4}$$

L_{e} is the magnetic path length, N_1 is the primary winding, N_2 is the secondary winding and A_{e} is the effective net core area of the steel sample.

Experiments were performed for flux densities from 0.2T to 1.4T at frequencies ranging from 50Hz to 300 Hz. Graphs were plotted for the change in relative permeability and core loss. The core losses were bifurcated into hysteresis and eddy current losses using the Steinmetz and Bertotti's model. The B-H curves are obtained from the B-H analyzer [32].

2.5 Results

The relative permeability, core loss, B-H curves, and current waveforms were obtained.

Comparison of B-H curves

The B-H curves of all four samples were compared using a B-H analyzer. Figure 2.5 shows the comparison of the B-H curves of all four samples at a magnetic flux density of 1.2T and a fixed frequency of 50Hz.

From the experiment performed, it was observed that the laser-jet unannealed sample had the maximum B-H curve area in comparison to the other samples which proved that it had the highest hysteresis losses. On the hand the water-jet sample had the least B-H curve area. The punch cut sample had a lesser B-H curve area in comparison to the laser-jet sample. In addition to the above observations, it was also noted that the sample that had the highest core loss had the highest coercivity and the least retentivity.

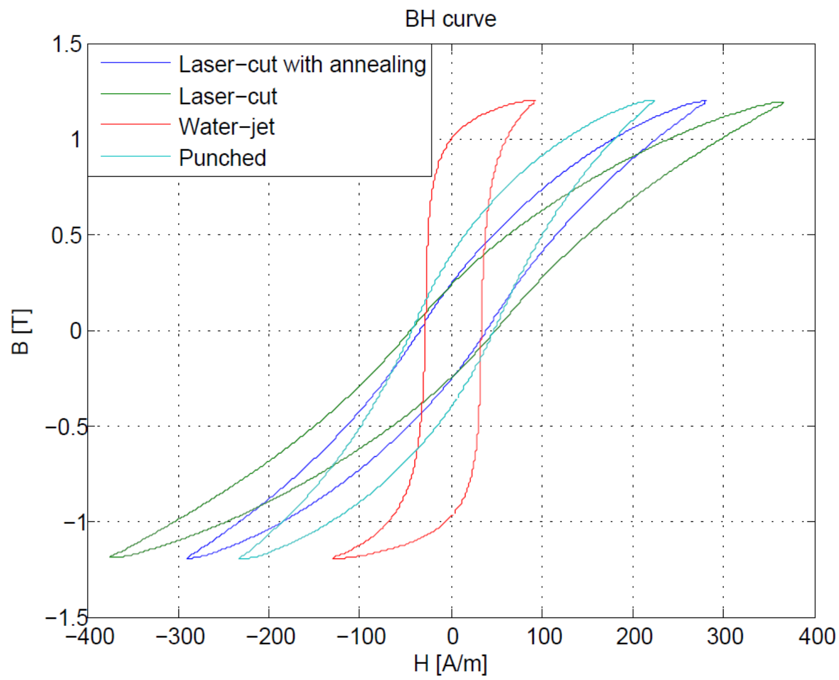

Figure 2.5. Comparison of B-H curves

On comparing the laser-jet samples before and after the annealing process, it was examined that there was a definite decrease in the hysteresis losses after the sample was annealed therefore exhibiting the importance of annealing.

Comparison of Core Loss

The core loss of different cutting samples were compared using the results from the B-H analyzer [32]. The results were noted by first varying the magnetic flux density and keeping the frequency constant and then varying the frequency at a fixed magnetic flux density. The core loss was divided into hysteresis and eddy current loss using the Steinmetz equation and Bertotti's model.

Figure 2.6 shows the measurements of core loss per unit volume of the ferromagnetic samples at a fixed frequency of 50Hz and a varying magnetic flux density from 0.2T to 1.4T.

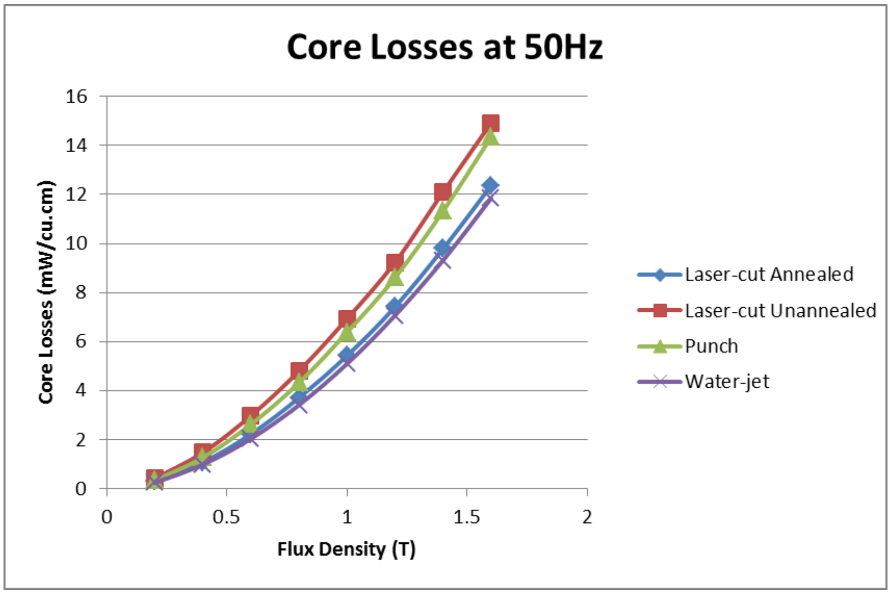

Figure 2.6. Variation of core loss per unit volume with respect to flux density for different cutting techniques

It was observed that the laser-jet unannealed sample exhibited the highest core loss per unit volume and the water-jet sample showcased the least core loss per unit volume. As expected through previous observation of the B-H curves, the annealing had a favorable influence on the magnetic properties of the core and the losses decreased after annealing.

Upon dividing the core loss into hysteresis and eddy current loss at 50Hz, it was observed that the core loss was dominated by the hysteresis loss at lower frequencies. Figure 2.7, shows the increase in hysteresis loss per unit volume with respect to the change in magnetic flux densities at 50Hz for the different cutting techniques.

Even at a lower frequency of 50Hz, the hysteresis loss per unit volume for Laser-cut unannealed sample was noted to be 16.03% higher than the Laser-cut annealed sample thereby stressing the importance of annealing.

In the next section, observations were noted at a fixed flux density and by varying the frequency of the pulse input. In Figure 2.8 the core loss per unit volume was studied at a fixed magnetic flux density of 0.2T and a changing frequency from 50Hz to 300Hz.

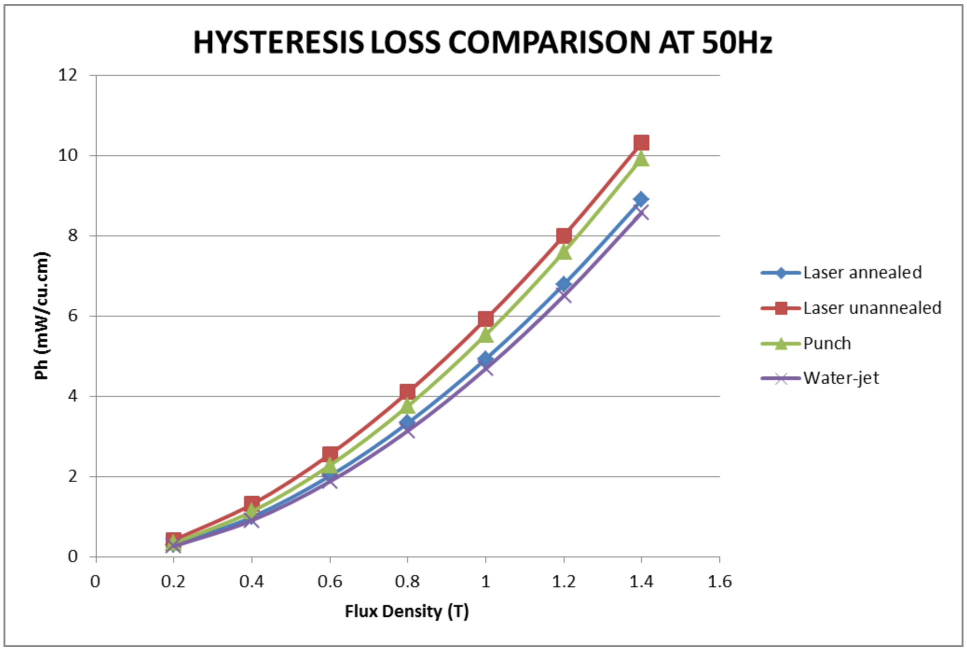

Figure 2.7. Comparison of hysteresis loss for different cutting techniques

It was observed that with increase in frequency, the core loss of all four samples increased. This was due to the higher eddy current loss. At a higher frequency, the core loss was dominated by the eddy current loss.

On further examination and mathematical calculation, it was noted that at 300Hz, the core loss per unit volume of the laser-cut unannealed sample was 33.95% higher than the water-jet sample.

As previously observed and noted, annealing improved the magnetic properties of the laser-jet sample. It was examined that at 300Hz the laser-jet unannealed sample had 28.27% higher core loss per unit volume in comparison to laser-jet annealed sample.

Comparison of Relative Permeability

Higher relative permeability in ferromagnetic cores is necessary to confine the magnetic field lines in the core. Therefore, while choosing the type of steel for the machine core, a ferromagnetic material of higher permeability is preferred.

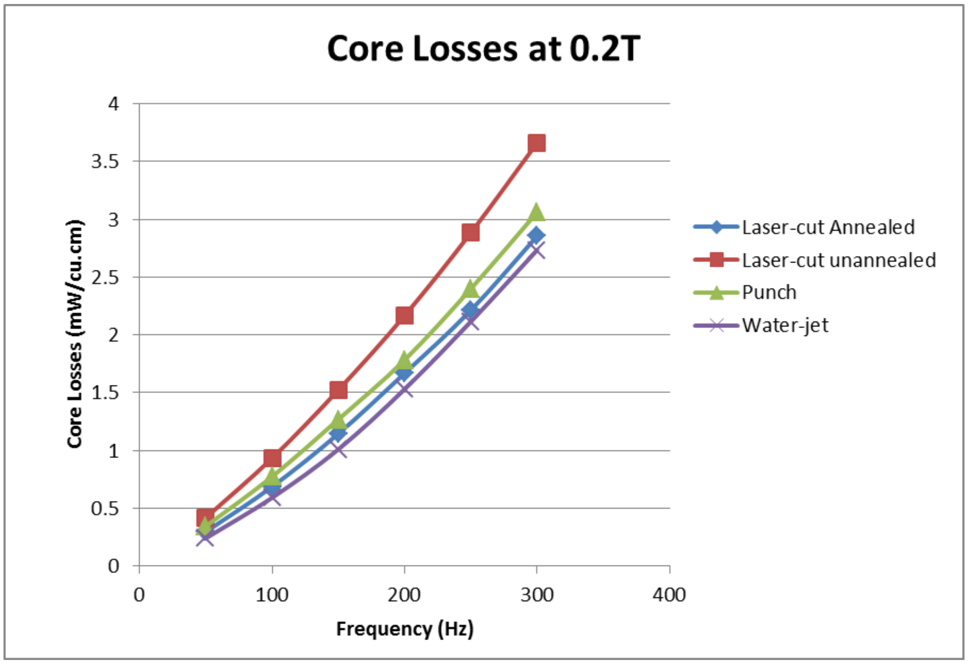

Figure 2.8. Variation of core loss per unit volume with respect to frequency for different cutting techniques

It is observed through experiments conducted that the different cutting techniques influences the relative permeability of the magnetic core material [32].

The relative permeability of the samples were obtained using the experimental process explained above. The results were compared by varying the magnetic flux density at a constant frequency. Figure 2.9 shows the measurements of relative permeability with respect to the magnetic flux density.

The water-jet sample was observed to have the highest permeability of 7000 at 0.4T. The punch sample had a maximum relative permeability of 4000 at 0.8T. Laser-jet unannealed sample had the a maximum permeability of approximately 2500 which was lesser than all the other magnetic steel samples.

The permeability of the laser-jet sample was improved by annealing. After annealing, the relative permeability increased to approximately 3200. Annealing was found to improve the permeability of the core material by approximately 28% at 0.4T.

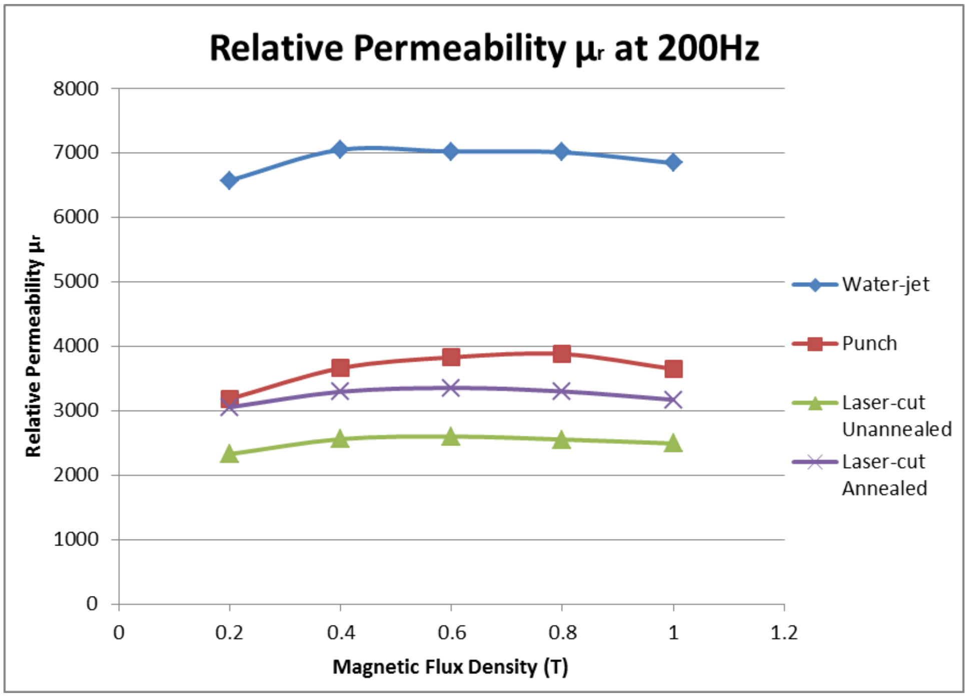

Figure 2.9. Variation of relative permeability with respect to flux density for different cutting techniques

2.6 Conclusion

Core loss estimation is an essential topic in electric motor design. The detrimental effects caused due to different cutting techniques is a well-established problem.

In this chapter, experiments were conducted to compare the effects of punch, laser-jet and water-jet cutting process on the magnetic properties of the ferromagnetic material. The effects of annealing on the magnetic properties of the core was also studied and results were compared.

Table 2.1 shows a summary of core loss per unit volume, hysteresis loss per unit volume, coercivity and relative permeability of magnetic materials cut by different techniques at a fixed frequency and flux density of 50Hz and 1.2T respectively.

Table 2.1. Loss, coercivity and relative permeability μ_r at 50 Hz and 1.2 T

Cutting type	P_c(mW/cm^3)	P_h(mW/cm^3))	H_c(A/m)	μ_r
Laser-cut unannealed	9.2351	8.0030	47.248	2555.9
Punch	8.6088	7.5980	45.061	4024.7
Laser-cut annealed	7.4165	6.7888	36.741	3327
Water-jet	7.2872	6.5031	30.789	8488.9

Under the same experimental conditions, it was found that laser-jet sample had the maximum core loss per unit volume and the least relative permeability in comparison to punch and water-jet samples.

Water-jet sample was found to have the least core loss per unit volume and maximum relative permeability thereby proving to be a reliable material for the machine core. It was also observed that upon annealing of the laser-jet sample, the electromagnetic properties of the core improved.

Thus, it can be concluded that water-jet cutting is the preferred technique for non-oriented steel and laser-jet cutting technique has the most detrimental effect on the magnetic properties of ferromagnetic material.

It can also be concluded that annealing of steel after the cutting process improves the magnetic properties of the ferromagnetic material.

CHAPTER 3

EFFECTS OF HYSTERESIS LOOP ON THE INDUCTIVE CIRCUIT

The previous chapter discussed about the influence of different cutting techniques and post annealing process on the magnetic properties of ferromagnetic material.

It was concluded that the different cutting techniques affected the B-H curve of the material along with its relative permeability and core loss. The water-jet cutting technique that had the least hysteresis loss had the least coercivity and highest retentivity. It could be observed that the B-H curve became less 'S-shaped' and more rectangular shaped as the hysteresis loss decreased.

This chapter discusses the influence of hysteresis loop or B-H curve of the ferromagnetic material on the machine performance. The Jiles-Atherton (J-A) model is applied to describe the dynamics of a linear and nonlinear circuit with a pulse voltage input comprising of a resistor and an inductor in series, whose core displays linear, saturation and hysteresis conditions.

Jiles and Atherton concluded through their works that all the stress induced changes observed move the state of magnetization towards the anhysteretic curve or energy minimization.

3.1 The Circuit

The magnetic flux in a ferromagnetic core material is analogous to the current flow in a conductor. For the magnetic flux to travel through the circuit, a force is required. This motivating force in the magnetic circuits is known as Magnetomotive force (mmf).

The mmf is related to the flux ϕ by a property of the ferromagnetic material known as the reluctance.

$$mmf = \phi\Re \tag{3.1}$$

The mmf required to produce the flux is supplied by the changing current through the coil. The mmf can be obtained by multiplying the number of turns of the coil and the amount of current through the coil. This current is also referred to as the magnetizing current.

A pulse voltage produces a triangular changing current. It is observed that the magnetizing current through a ferromagnetic core inductor is not always perfectly triangular due to the nonlinear saturation and hysteresis effects of the core.

In order to discuss the effects of non-linearity on the magnetizing current and therefore on the magnetic flux, a simple non-linear circuit with a resistor and inductor in series that displays the saturation and hysteresis behavior was simulated.

The circuit that was modelled is known as a ferroresonant circuit [21]. Figure 3.1 [21] shows a model ferroresonant circuit. This circuit model will also be helpful in studying the influence of nonlinear inductors present in many power electronic circuits whose core saturates and displays hysteresis.

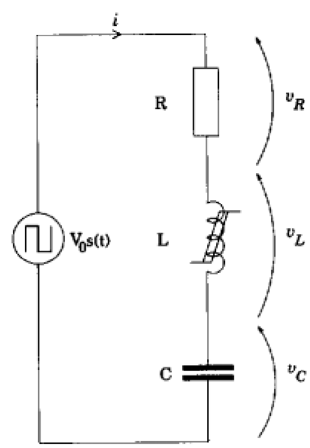

Figure 3.1. Ferroresonant Circuit (Source: Deane, J. H. (1994). Modeling the dynamics of nonlinear inductor circuits. IEEE Transactions on Magnetics 30 (5), 27952801.)

Referring to Figure 3.1, the resistor used in the circuit was linear and capacitor was not included in the simulation in order to mimic a simple machine model.

For the simulations that will be discussed below, the resistance was fixed at $R = 0.1\Omega$. The inductor core had an area of cross-section, $A = 70$ x 10^{-6} m^2. The winding had 700 turns and the magnetic path length of the core was $l_{\mathrm{m}} = 25$ x $10^{-2}m$. The voltage input was a pulse wave of 20V amplitude at a frequency of 50Hz.

3.2 Saturation and Hysteresis modeling using Jiles-Atherton Model of Ferromagnetic Hysteresis

Jiles and Atherton proposed a first-order non-linear differential equation to study the non-linearity in ferromagnetic core materials based on the magnetization process [27].

The solution of the equation could be numerically solved to give the magnetization, M, in terms of the external magnetic field, H. The differential equation is as follows:

$$\frac{dM(H)}{dH} = (1-c)\delta_{\mathrm{M}}\frac{M_{\mathrm{an}}(H_{\mathrm{e}}) - M(H)}{k(1-c)sign(\dot{H}) - \alpha[M_{\mathrm{an}}(H_{\mathrm{e}}) - M(H)]} + c(\frac{\partial M_{\mathrm{an}}(H_{\mathrm{e}})}{\partial H})_{\mathrm{M}} \tag{3.2}$$

The two step functions sign(.) and δ_{M} are defined as shown below:

$$sign(x) = \begin{cases} 1, & \text{if } x \geq 0 \\ -1, & \text{otherwise} \end{cases} \tag{3.3}$$

and

$$\delta_{\mathrm{M}} = \begin{cases} 0, & \text{if } \dot{H} < 0 \text{ and } M_{\mathrm{an}}(H_{\mathrm{e}}) - M(H) \geq 0 \\ 0, & \text{if } \dot{H} \geq 0 \text{ and } M_{\mathrm{an}}(H_{\mathrm{e}}) - M(H) \leq 0 \\ 1, & \text{otherwise} \end{cases} \tag{3.4}$$

Here c is the ratio of initial normal to initial anhysteretic differential susceptibility; α is the mean field parameter representing the domain coupling; k is a measure of hysteresis in A/m. $ksign(h)$ gives the width of the hysteresis loop, and when $k = 0$, no hysteresis is present.

$M_{\mathrm{an}}(H_{\mathrm{e}})$ is the anhysteretic magnetization function that determines the shape of the hysteresis curve. It is represented by a Langevin function as follows:

$$M_{\mathrm{an}}(H_{\mathrm{e}}) = M_{\mathrm{s}}[coth(H_{\mathrm{e}}/a) - (a/H_{\mathrm{e}})] \tag{3.5}$$

M_{s} denotes the the magnetic saturation in A/m and a is the scaling factor in A/m [27].These parameters were used to model the B-H curves for the ferroresonant circuit given in Figure 3.1.

3.3 Mathematical Equation for the Circuit

The differential equation of the circuit was derived using the Jiles-Atherton equations.

According to Kirchhoff's voltage law:

$$V(t) = V_{\mathrm{R}} + V_{\mathrm{L}} \tag{3.6}$$

where $V(t)$ is the input pulse voltage. The resistor and inductor voltages are V_{R} and V_{L} respectively.

$$V_{\mathrm{R}} = IR \tag{3.7}$$

where I is the input current and R is the resistance of the circuit.

The value of V_{L} changed with conditions of linearity, saturation and hysteresis.

In the case of a linear inductor circuit:

$$V(t) = IR + L\frac{dI}{dt} \tag{3.8}$$

When saturation of the inductor core was taken into consideration, the inductance of the circuit was assumed to be current dependent and the circuit equation shown below was used in the MATLAB Simulink model:

$$V(t) = IR + L(I)\frac{dI}{dt} \tag{3.9}$$

Upon hysteresis, Jiles-Atherton model and Ampere circuital law was used to derive the inductor voltage.

According to [27], the inductor voltage could be represented as:

$$V_{\mathrm{L}} = \mu_0 nA\frac{d}{dt}(H+M) = \frac{\mu_0 nAH}{I}\frac{dI}{dt}[1+\frac{dM}{dH}] \tag{3.10}$$

The value of $\frac{dM}{dH}$ was obtained from equation 3.2. By substituting 3.10 in equation 3.6, the non-linear magnetizing current due to non-linear B-H magnetization curve of the ferromagnetic core was obtained.

$$\frac{dI}{dt} = \frac{I}{\mu_0 nAH}\frac{V(t)-IR}{1+\frac{dM}{dH}} \tag{3.11}$$

The magnetizing current under all three conditions of linearity, saturation and hysteresis were compared using MATLAB Simulink model to showcase the effects of saturation and hysteresis on the ferroresonant circuit.

3.4 MATLAB Simulation

MATLAB Simulink [37] was used to model the ferroresonant circuit. Three different circuits were simulated based on equations 3.2, 3.9 and 3.10. B-H curves were derived using the Jiles-Atherton model.

The parameters for the model were obtain by non-linear least square method [29]. The parameters are summarized in Table 3.1.

Table 3.1. Jiles-Atherton Parameters

M_s	1.6×10^6 A/m
a	1100 A/m
k	400 A/m
α	1.6×10^{-3}
c	0.20

The simulink model was incorporated with all the three conditions of linearity, saturation and non-linear hysteresis to compare the magnetizing current waveforms and showcase the effects of saturation and hysteresis on the circuit.

3.5 Results

The first circuit was simulated using a linear resistor and a linear inductor. Figure 3.2 shows the input pulse voltage of 20V and triangular magnetizing current in the absence of saturation and hysteresis.

It was observed that the magnetizing current produced was a perfect triangular waveform with amplitude of 7A. Jiles-Atherton model was used to create the B-H curves in the simulation. Figure 3.3 shows the saturation B-H curve.

It can be observed that due to the Jiles-Atherton parameter M_s, the material saturates at approximately 2T.

Figure 3.4 shows the hysteresis B-H curve formed with respect to the Jiles-Atherton parameters chosen. The hysteresis curve also shows the initial susceptibility which is the point at which the magnetization is reversible.

The saturation and hysteresis magnetizing currents were obtained using the equations 3.9 and 3.10. It was observed that the current waveforms were no longer triangular in both the saturation and hysteresis case.

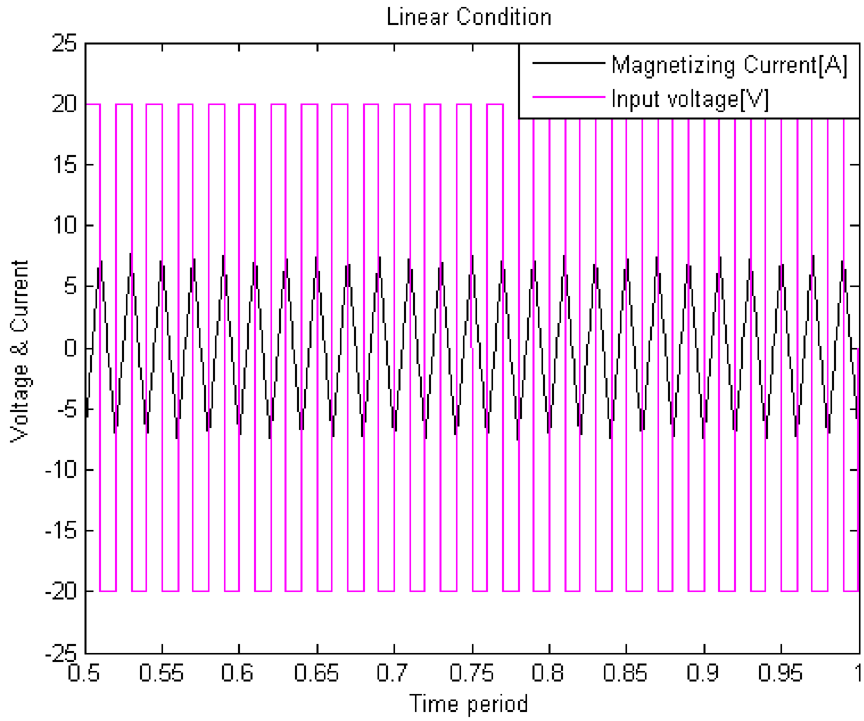

Figure 3.2. Magnetizing Current under Linear condition

The magnitude of the magnetizing current was also greater than the linear case. This was because, now more current was required to produce the mmf that would give the required flux. Figure 3.5 shows the comparison of magnetizing currents under linear, saturation and hysteresis conditions. It can be clearly observed that hysteresis magnetizing current was highly non-linear with a maximum magnitude of 10A. Therefore, it can be concluded that the B-H saturation and hysteresis of ferromagnetic core material affects the performance of the circuit.

3.6 Conclusion

MATLAB modelling of a simple R-L circuit was conducted to note the change in current waveforms under different conditions of linearity, saturation and non-linear hysteresis.

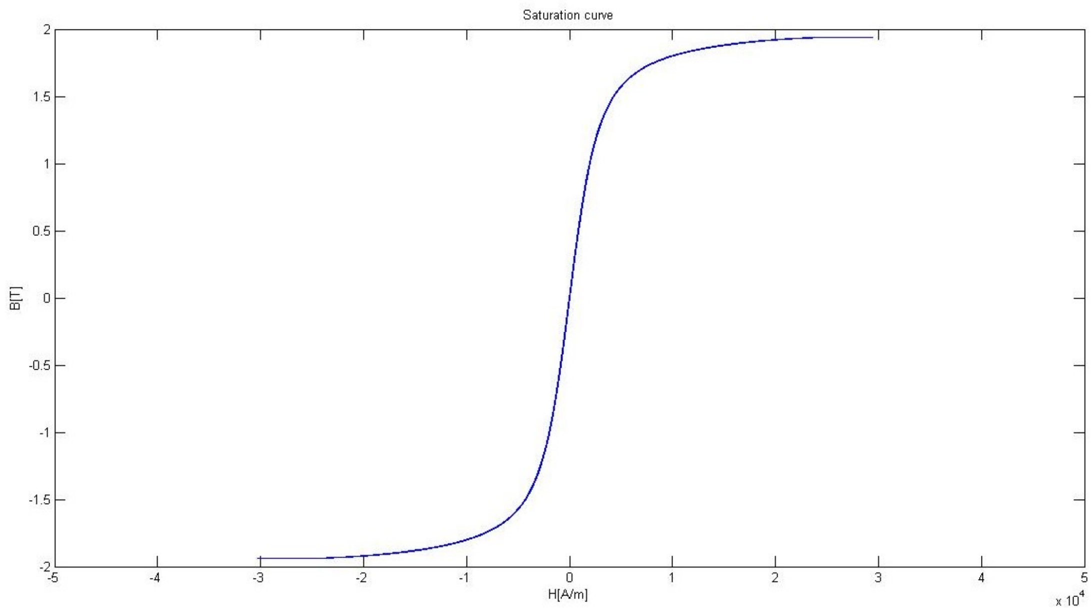

Figure 3.3. Saturation B-H curve

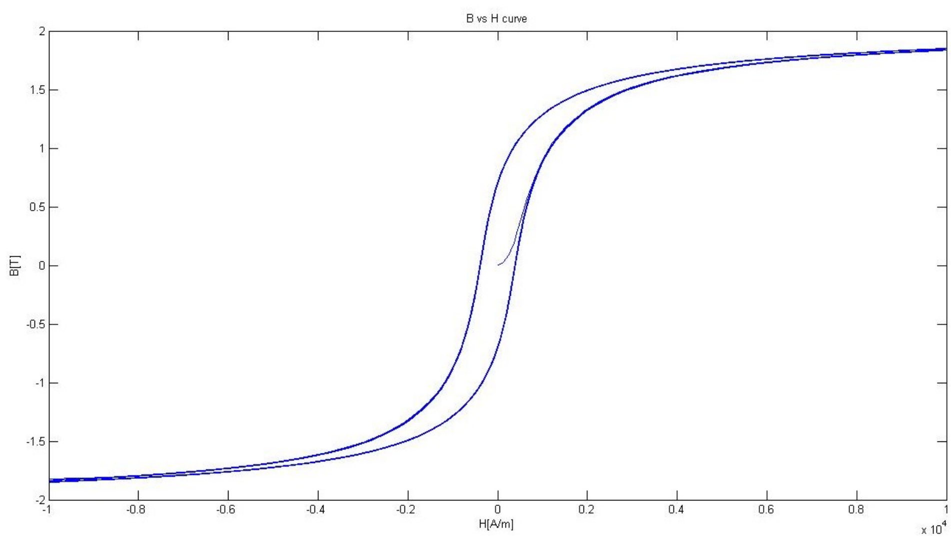

Figure 3.4. Hysteresis B-H curve

It was observed that during the linear condition the current waveform was perfectly triangular with a maximum value of approximately 7A. During the saturation and non-linear hysteresis conditions, the magnitude of the current waveform increases but the waveform is observed to deviate from the triangular shape.

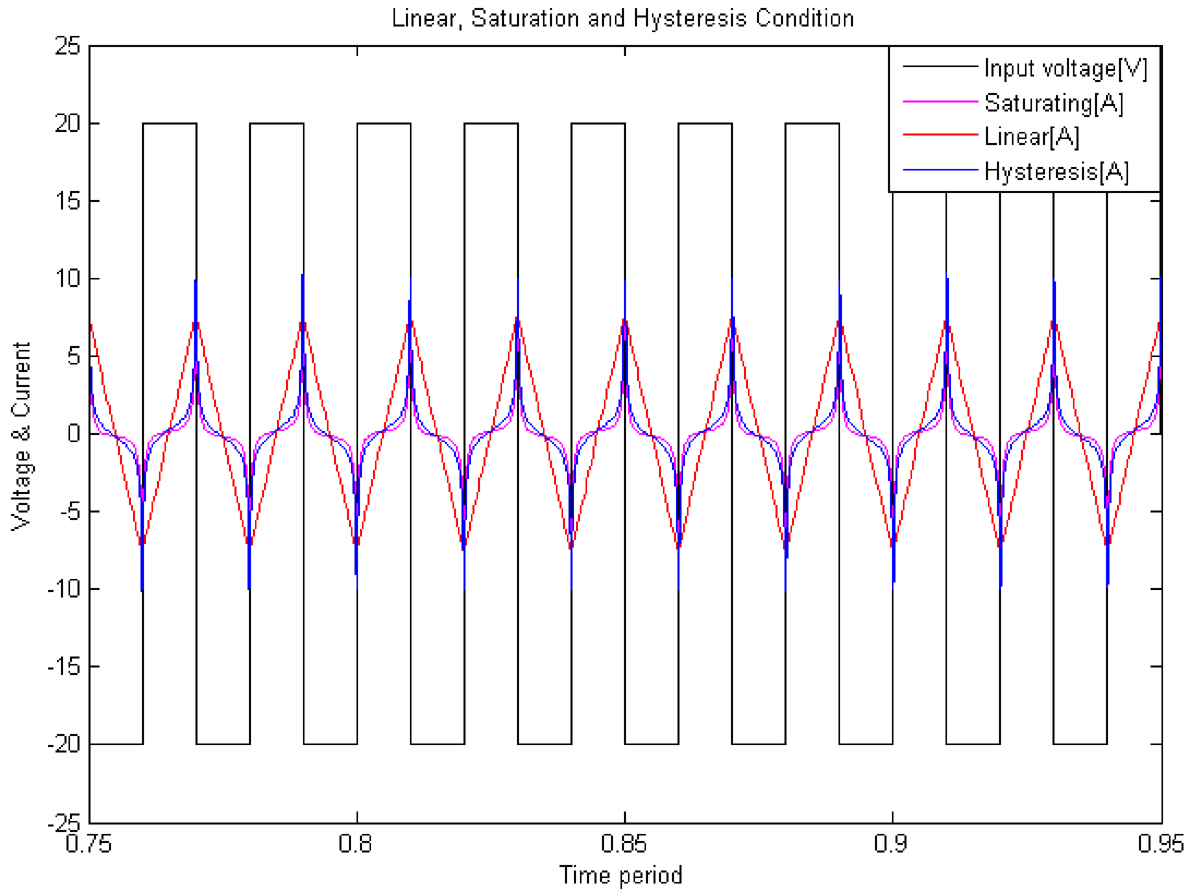

Figure 3.5. Magnetizing Current under Linear, Saturation and Hysteresis condition

Therefore, it can be concluded that the B-H curve of magnetic steel affects the current waveform of a machine thus affecting the overall performance of the machine.

CHAPTER 4

AIR-GAP LENGTH IRREGULARITIES DUE TO CUTTING PROCESSES

The previous two chapters discussed about the influence of cutting techniques on the B-H curve, core loss and permeability of ferromagnetic materials and the effects of B-H curve on the magnetizing current and machine performance.

This chapter mainly focuses on the surface irregularities due to the different cutting techniques that was introduced and discussed in Chapter 2. It highlights important aspects of surface finishes that affects the power density and torque characteristics in a machine.

4.1 Surface Imperfections

As discussed, the laminations of core used in electric machines are cut using punch, laser-jet and water-jet techniques. Previous research showed that the cutting techniques affected the surface finish especially the edges of the laminations.

Schoppa [45] discussed the influence of punching and laser-jet cutting on the magnetic properties of non-oriented magnetic steel. Moses [40] talked about the aspects of the cut-edge stress on the power loss and flux density distribution in electrical steel sheets. In [35], Loisos examined the effects of mechanical and Nd: YAG laser cutting on magnetic flux distribution near the cut edge of non-oriented steels.

But past research did not focus on comparing the surface imperfections of commonly used cutting techniques and post annealing processes.

The research and experiments conducted in this thesis focuses on comparing the surface imperfections due to the punch, laser-jet and water-jet cutting techniques. It also studies the improvements observed in the cutting surfaces due to post annealing process.

In addition, it examines the effects of surface imperfections on the machine performance characteristics such as power density and torque.

4.2 Effect of Air-gap on the Performance of Machines

The distance between the stator and rotor core is known as the air-gap of the machine. The air-gap has effects on the performance of the machine, and is generally required to be kept as small as possible because a larger air-gap may be a source of lower power factor. Very small air-gaps may cause mechanical issues such as noise and losses.

In electric machines, power is produced by the magnetic flux that passes through the air gap which has very low permeability. Air-gap length between the stator and rotor is an important factor that also influences the torque production in a machine. A higher air-gap requires more magnetizing current to produce the mmf. This leads to higher winding losses which affects the performance of the machine.

In case of an Interior Permanent Magnet Synchronous machine (IPMSM), the permanent magnets present in the rotor have a permeability value equal to that of air, and acts like an air-gap along the d-axis of the rotor. A change in the air-gap length in case of an IPMSM machine will not have much significance along the d-axis but will affect the inductance along the q-axis. An increase in air-gap will lead to a decrease in inductance along the q-axis [49].

It is therefore necessary to understand the effects of the manufacturing processes on the surface finish of the magnetic materials especially those used in cores of machines. In observations described in following sections, it is noted that different cutting techniques may cause mechanical damage or surface abrasions which may result in increase in air-gap when used as laminations for electric machines.

Comparisons were made in order to note the manufacturing process that may have a lesser detrimental effect on the performance of the machine.

4.3 Experimental Observation

A digital microscope with 2-D and 3-D imaging capabilities was used to study the surface imperfections of the laminations.

4.3.1 Digital Microscope

A VHX-5000 Keyence Digital Microscope was used to study the surface finish of the laminations [3]. The HDR function of the microscope was used to gather additional color information to render a detailed image since the samples had low color gradation.

Depth composition function was used to view the complete sample in focus in spite of the significant height variations in some samples. The samples were viewed at a scale of 10μm since air-gap variation of even 100μm was known to have a significant impact on the performance of machines.

The 3-D display function was used to view the crevice depth of each lamination and the measurement function was used to measure the irregularities of each lamination. The light shift function was used to enhance the height variations by altering the angle of lighting.

4.3.2 Results

The surface finish of all four laminations were observed through the digital microscope and the following results were obtained.

Punch-Cut Sample

Figure 4.1 shows the 2-D image of the punch-cut sample.

It was observed that the edges of the punch laminations were found to be highly damaged.

This could also affect the performance of the machine. 3-D image was captured using the digital microscope to observe the possible additional air-gap or crevice depth due to the imperfect surface finish of the sample.

Figure 4.2 shows the 3-D microscopic image of the punch-cut sample. From the figure, it could be examined that the punch-cut sample had a maximum crevice depth of 43.12 μm. The crevice was found at the border of each lamination.

Figure 4.1. 2-D Image of Punch-Cut Sample

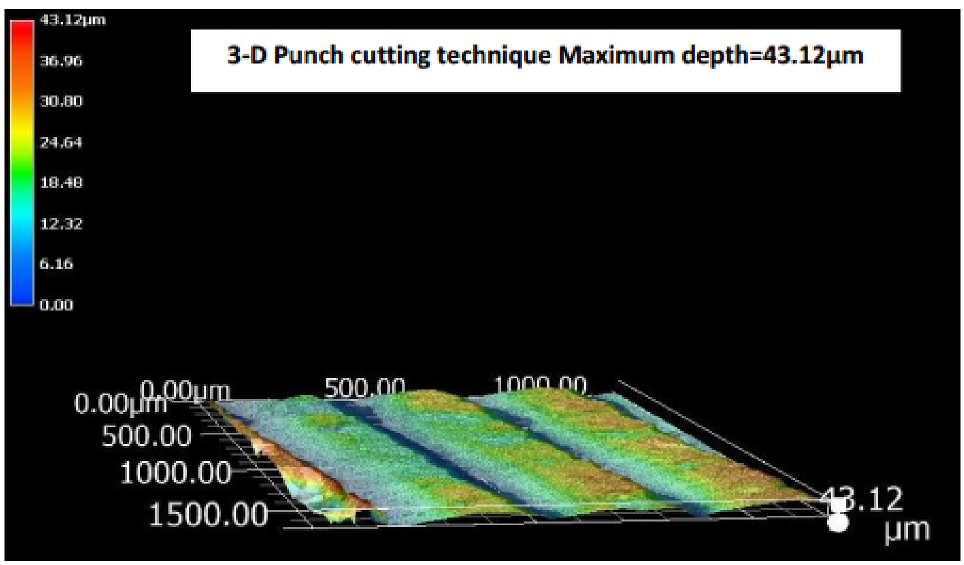

Figure 4.2. 3-D Image of Punch-Cut Sample

Laser-Jet Unannealed Sample

Laser-jet unannealed lamination sample was observed under the digital microscope. Figure 4.3 and Figure 4.4 shows the 2-D and 3-D images of the sample respectively.

It was observed that the laminations had a maximum crevice depth of 146.49 μm. As previously observed, the crevice was found to be at the edges of the laminations.

In comparison to the punch sample that was discussed, although the edges of the laminations werent as damaged, but the crevice depth was much larger. This could be one of the reasons for a higher core loss in comparison to the punch sample.

This factor might play a crucial role while designing cores for electric machines as it may be responsible for increasing the air-gap between the stator and the rotor-core.

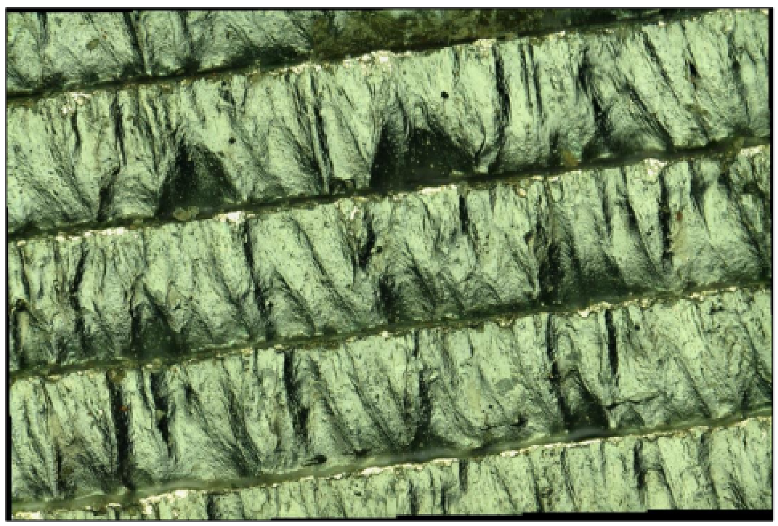

Figure 4.3. 2-D Image of Laser-Jet Unannealed Sample

Laser-Jet Annealed Sample

Chapter 2 of the thesis discussed the benefits of post-annealing process on the laminations. It was found that annealing increased the relative permeability and decreased the core loss of the machine.

The surface finish of the laser-jet annealed sample was compared with the unannealed sample to note the benefits of post-annealing processes.

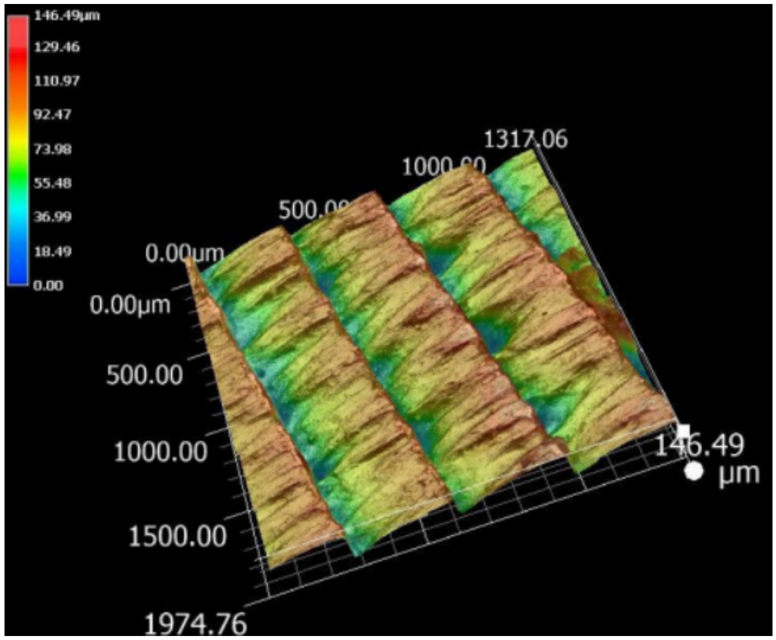

Figure 4.4. 3-D Image of Laser-Jet Unannealed Sample

Figure 4.5 and Figure 4.6 shows the 2-D and 3-D images of the annealed sample respectively. It was noted that the maximum crevice depth or surface imperfection decreased from 146.49μm to 129.46μm.

Figure 4.5. 2-D Image of Laser-Jet Annealed Sample

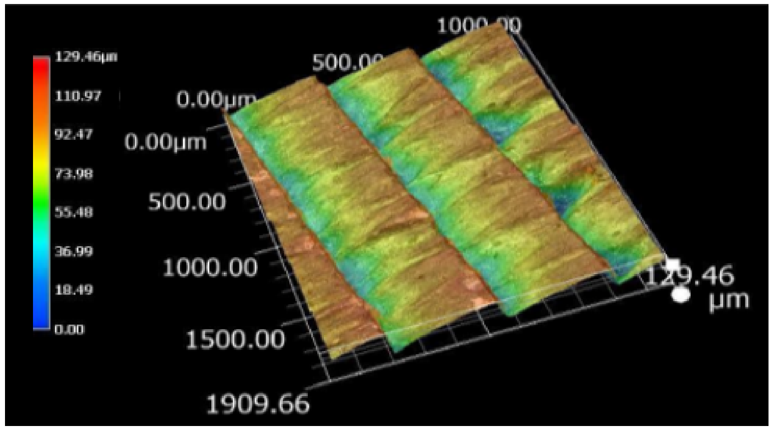

Figure 4.6. 3-D Image of Laser-Jet Annealed Sample

The surface of the laminations was also found to be smoother in comparison to the laser-jet unannealed sample. Although, in comparison to the punch cut sample, the crevice depth was still higher.

Water-Jet Sample

In Chapter 2 it was discussed that the water-jet sample was found to be the most suitable since it had the highest relative permeability and the least core-loss.

The laminations of the water-jet sample were also observed under the digital microscope and was compared with other lamination samples.

Figure 4.7 and Figure 4.8 shows the 2-D and 3-D images of the annealed sample respectively. It was noted that the maximum crevice depth or surface imperfection was much lesser than all the other samples.

It was found that, in comparison to punch, laser-jet unannealed and laser-jet annealed sample, water-jet sample had the least imperfection. The maximum crevice depth was found to be 41.78μm for each sample.

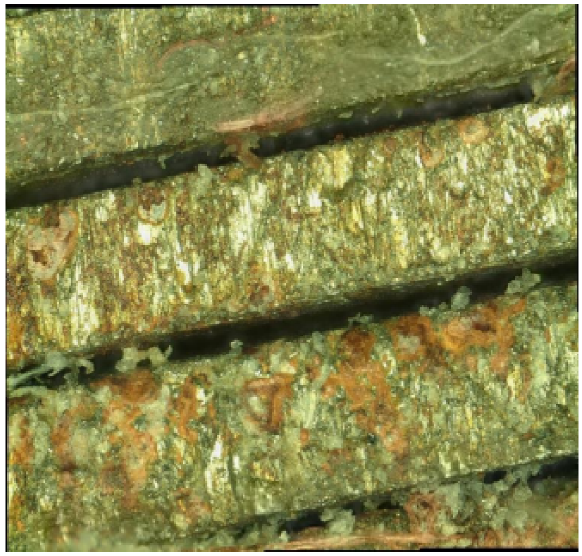

Figure 4.7. 2-D Image of Water-Jet Sample

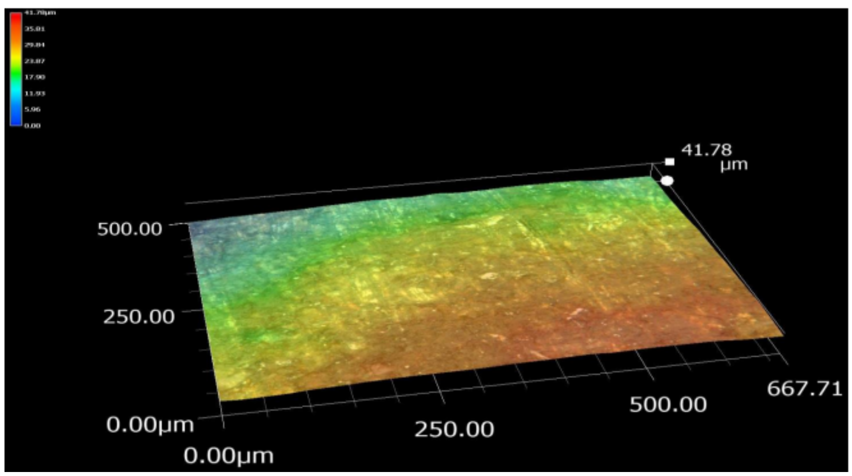

Figure 4.8. 3-D Image of Water-Jet Sample

4.4 Conclusion

The different samples which were cut by punching, laser-jet cutting and water-jet cutting technique were observed under a digital microscope in order to understand the effects of the manufacturing processes on the surface finish of the material.

It was noted that a higher abrasion or crevice depth could cause a larger air-gap when used as cores in electric machines.

It was observed that the laser-jet sample had the highest crevice depth and the water-jet sample had the least crevice depth. When annealing was performed after the cutting process, the surface finish of the magnetic materials improved and the crevice depth was reduced to a lower value.

Therefore, it could be concluded that water-jet cutting technique was a better choice in comparison to laser-jet and punch cutting techniques and caused lesser detrimental effects. It could also be concluded that post-annealing process improved the surface finish of laminations.

CHAPTER 5

EFFECTS OF HIGH-ENERGY MAGNETS ON THE PERFORMANCE OF PERMANENT MAGNET SYNCHRONOUS MACHINES

Previous chapters of the thesis discussed in detail about the effects of manufacturing processes on the magnetic properties and surface finish of ferromagnetic materials.

This chapter examines the effects of high-energy magnets used in Permanent Magnet Synchronous Machines (PMSM) on the ferromagnetic core material especially the rotor core which is also of paramount importance for the performance of the machine.

5.1 Introduction

PMSM and induction motors (IM) are extensively used for diverse applications. Although the use of IM is on the rise due to cost inconsistency in high-energy magnets, PMSM motors are still preferred due to their compact size, high power density, and efficiency.

In interior permanent magnet synchronous motor (IPMSM) and surface mounted permanent magnet synchronous motor (SPMSM), the magnetic steel rotor core is in permanent contact with the high-energy magnets. This chapter discusses the effects of these high-energy permanent magnets on the magnetic properties of magnetic steel core.

Through the experiments conducted, it is examined that the relative permeability of the ferromagnetic core decreases when it is kept in contact with three sintered Neodymium (NdFeB), grade N45 permanent magnet.

Simulations are performed to show the effects of relative permeability on the machine performance of an IPMSM motor. It therefore characterizes a very critical concept which is typically ignored while designing motors.

5.2 Theory

The below sections describes two important factors that might be responsible for the high-energy magnets to change the magnetic properties of the magnetic steel sample.

5.2.1 Demagnetizing Fields

A magnetic field can be produced by either applying current to a conductor or using magnetic poles [18]. If the field is produced using current, closed loop magnetic lines are formed. If the magnetic lines are formed using magnetic poles, the field lines begin at the north pole and end at the south pole.

If a sample is magnetized by a field from left to right, then the north pole is formed on the right and the south pole is formed on the left side of the sample as shown in Figure 5.1. [18].

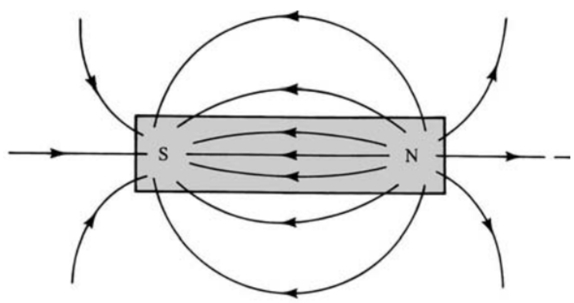

Figure 5.1. Magnetic field lines in Sample bar magnet (Source: Cullity, B. D. and C. D. Graham (2009c). Experimental Methods, pp. 23-86. Wiley-IEEE Press.)

It can be observed that some magnetic field lines are also observed to move from north to south pole inside the bar magnet. This tends to demagnetize the magnet. It is found to be in opposite direction to that of magnetization.

It is found that the field lines and flux density are found to diverge at the edges of the sample. This is due to the the fact that the demagnetizing field is greater at the poles than at the center of the sample [18]. In addition to the geometry of the sample, the demagnetization factor may also depend on the permeability and susceptibility of the sample. When the high-energy magnets are kept in contact with the magnetic steel, it might have caused an increase in the demagnetizing fields at the poles which in turn led to the decrease in permeability.

When the polarities of the magnets were changed in one of the cases discussed in section 5.4, the demagnetizing field may have decreased at the poles which helped the magnetic steel regain its magnetic properties and thus increase the permeability.

5.2.2 Effect of Soft magnetic material on Magnetic field

It is a known fact that when a soft magnetic material is placed in a existing magnetic field, the shape of the parallel field lines are altered. The flux lines tend to move towards the magnetic material as it is more permeable in comparison to the air. Figure 5.2 [18] shows the effect of a magnetized soft magnetic sample in a uniform field.

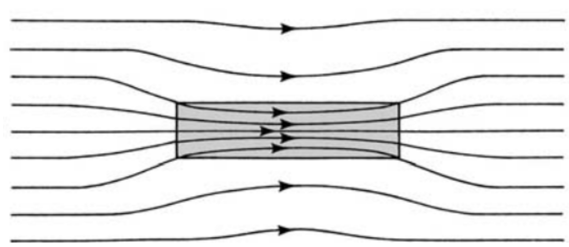

Figure 5.2. Magnetized body in uniform field (Source: Cullity, B. D. and C. D. Graham (2009c). Experimental Methods, pp. 23-86. Wiley-IEEE Press.)

Since the high energy magnets form uniform field lines, the flux lines tend to crowd towards the center of the magnetic steel sample. This may be another factor that is responsible for the change in magnetic properties.

A third reason may be the change in crystal lattice structure due to the presence of high-energy magnet. As discussed in previous chapters, a single crystal of iron has the easy magnetization direction of [100]. This may be also affected due to the strong magnetization caused due to the presence of the high-energy magnets.

The experiments performed in the next section focuses on the observations made after prolonged experiments were conducted using M-19 silicon steel and NdFeB high-energy magnets.

5.3 Experimental Setup and Process

5.3.1 E-core description

In the experiments performed, three samples of M-19 cores made with different cutting techniques used for previous experiments mentioned in Chapter 2 were reused. The punch, annealed laser-jet and unannealed laser-jet samples are represented as Sample 1, Sample 2, and Sample 3 respectively [44].

Each E-core sample was arranged in the same way as mentioned in Chapter 2. The purpose of using three samples for this experiment was to have more data points under varied conditions. Different criteria were examined.

All three cores used, consisted of 28 pieces of 29 gauge M-19 laminations. The E-cores were formed by welding the stack of laminations. Two coils of 300 turns were wound around the center leg of each E-core sample to create primary and secondary windings for the B-H analyzer.

The magnetic center path length was measured to be 228.6 mm and the cross-sectional area of the middle leg was 124.46 mm^2 for each sample. These dimensions were used as inputs in the B-H analyzer during analysis.

5.3.2 High-energy Magnets

Three sintered Neodymium (NdFeB), grade N45 high-energy permanent magnets were used for the experiment [44]. Table 5.1 shows the details of the magnets used for the experiment.

Table 5.1. Details of High-energy magnets

Material	Sintered neodymium rare earth magnet
Size	3/4”x3/4”x1/8”
Gauss rating	13,500 Gauss
Pole orientation	Magnetized through the thickness, the poles are on the 3/4” x 3/4” surfaces.
Tolerance	+/- 0.002 in

5.3.3 Experimental Setup

The samples were tested on a B-H analyzer. The setup and working of the B-H analyzer are explained in Chapter 2. The experimental setup was used to determine the relative permeability under different conditions.

5.3.4 Experimental Process

The E-core samples were kept in contact with the magnets for four weeks and measurements were taken every week to observe the change in magnetic properties of the cores, using the described B-H Analyzer. Figure 5.3 shows the test object with three Neodymium magnets.

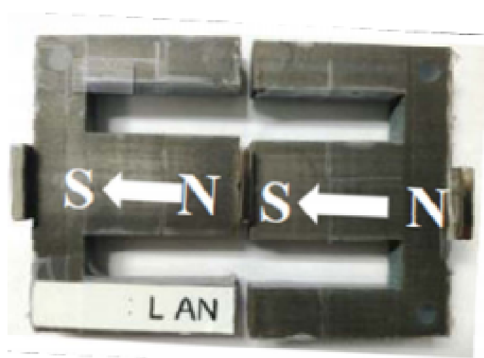

Figure 5.3. Illustration of the Sample with High-Energy Magnets

The magnets were placed with careful consideration of the orientation to allow the flux to pass through the core material. The experiment was performed for flux densities from 0.2 T to 1 T at frequencies ranging from 50 Hz to 300 Hz. Graphs were plotted to observe the change in relative permeability [44].

5.4 Experimental Results

The relative permeability and B-H curves were obtained using the B-H analyzer. The samples were tested under three different test conditions.

Case 1: Polarity Reversal

Figure 5.4 shows relative permeability of Sample 1 with respect to the magnetic flux density at 50 Hz observed for a time period of four weeks.

It was observed that during the first three weeks of the experiment, the relative permeability of the ferromagnetic core decreased due to the presence of high-energy magnets. The reduction was less significant at higher flux densities [44].

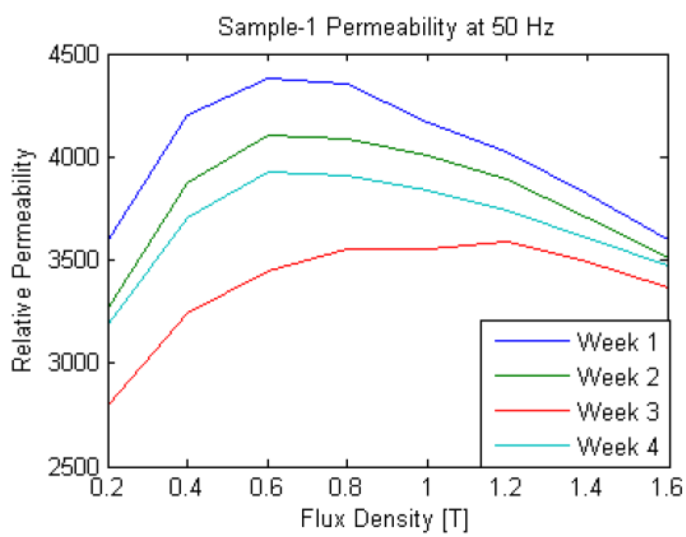

Figure 5.4. Change in Relative Permeability of Sample 1 at 50Hz

Before the fourth week of the experiment, the polarities of the magnets were reversed. This was done to observe if the ferromagnetic core regained its magnetic properties upon reversal.

The core was observed to get magnetized at the opposite direction and the ferromagnetic core regained its magnetic properties. The permeability increased during the fourth week. The core loss was measured and was approximately constant in all the cases.

Case 2: Influence of High-Energy Magnets for Four Week Experimental Period

For Sample 2, the permanent magnets were kept in contact with the ferromagnetic core for a four-week period. At the end of every week, observations were noted to examine the effects of the magnet on the steel core. It was observed that at the end of the fourth week, there was a 15% decrease in the relative permeability of the ferromagnetic core [44].

Figure 5.5 shows the change in relative permeability of Sample 2 with respect to the magnetic flux density at 50 Hz. It was observed, as expected, that the relative permeability gradually decreased during the four-week test period. Figure 5.6 shows the comparison of B-H curves of all four weeks at 50 Hz and 0.2T.

The area of the B-H curves remained approximately equal. In 5.6, it was observed that week-4 had the maximum coercivity and minimum retentivity in comparison to week-1.

Case 3: Observations after removal of magnets

In the case of Sample 3, the ferromagnetic core was exposed to the magnet for a four-week period as performed in previous cases. At the end of the fourth week, the magnets were removed. This was done in order to examine if the magnetic properties of the magnetic steel core could be regained [44].

At the end of the fifth week, it was observed that the core regained its magnetic properties. The value of the relative permeability was approximately equal to that of week-1. Figure 5.7 shows the change in relative permeability with respect to changing flux density at a frequency of 50 Hz.

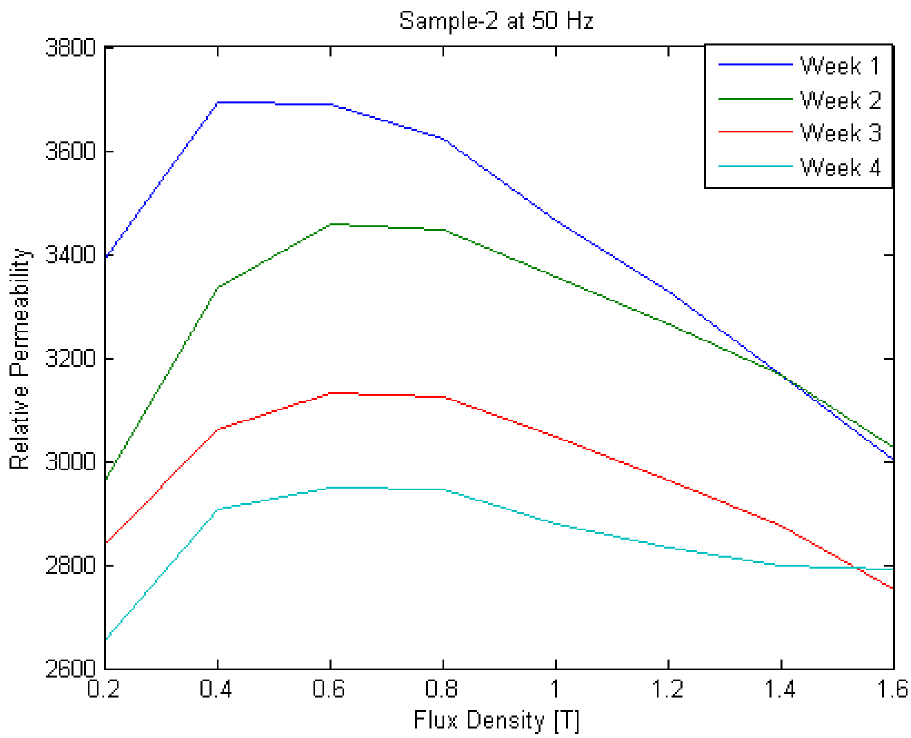

Figure 5.5. Change in relative permeability of Sample 2 at 50 Hz

It was observed that during the first four weeks, the relative permeability decreased as expected due to the influence of the high-energy magnets and at the end of the fifth week, the core regained its magnetic properties when it was separated from the high-energy magnets.

Effect of Increase in frequency

By examining the experimental results, it was noted that at higher frequencies the influence of high-energy magnets on the relative permeability of magnetic core was much less in comparison to lower frequencies.

The observation at lower frequency of 50 Hz and higher frequency of 300 Hz was noted down for each sample to emphasize that the effects of the high-energy magnets was dominated by the effects of increased frequency at 300 Hz. Table 5.2 shows the change in relative permeability at 50 Hz and 300 Hz [44].

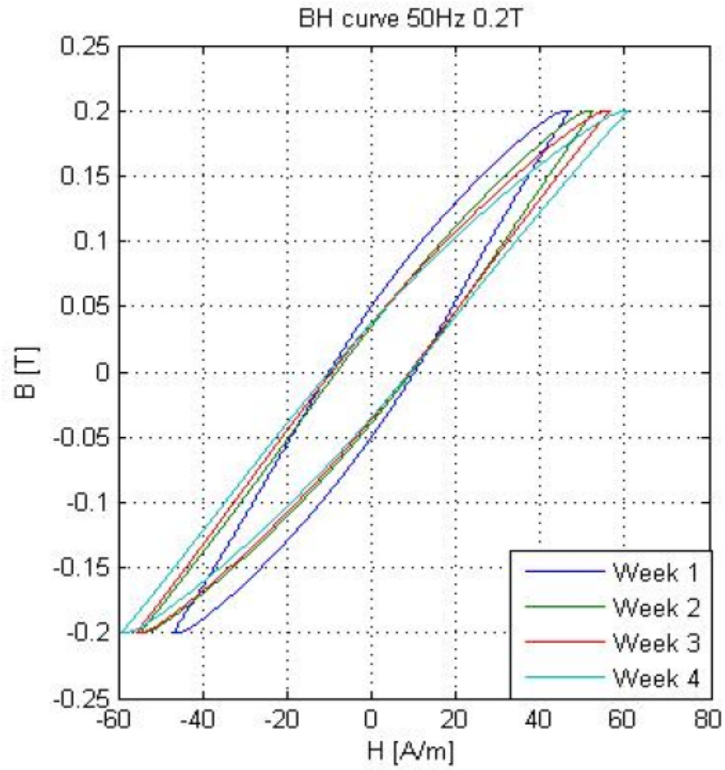

Figure 5.6. Comparison of B-H curves of Sample 2 at 50Hz and 0.2T

Table 5.2. Change in Relative Permeability of M-19 Samples at 50 Hz and 300 Hz

M-19 core sample	Frequency [Hz]	Flux density [T]	Initial μ_r	% decrease in μ_r
Sample 1	50	0.6	4380.1	21.34%
	300	0.6	3704.6	16.60%
Sample 2	50	0.6	3690.8	15.17%
	300	0.6	3116	8.60%
Sample 3	50	0.6	2790.8	15.69%
	300	0.6	2454	11.16%

It can be clearly observed from Table 5.2 that with the increase in frequency the influence of the magnets on the magnetic properties of ferromagnetic core decreased substantially. Hence, it could be concluded that frequency also plays a major role in IPMSM machines.

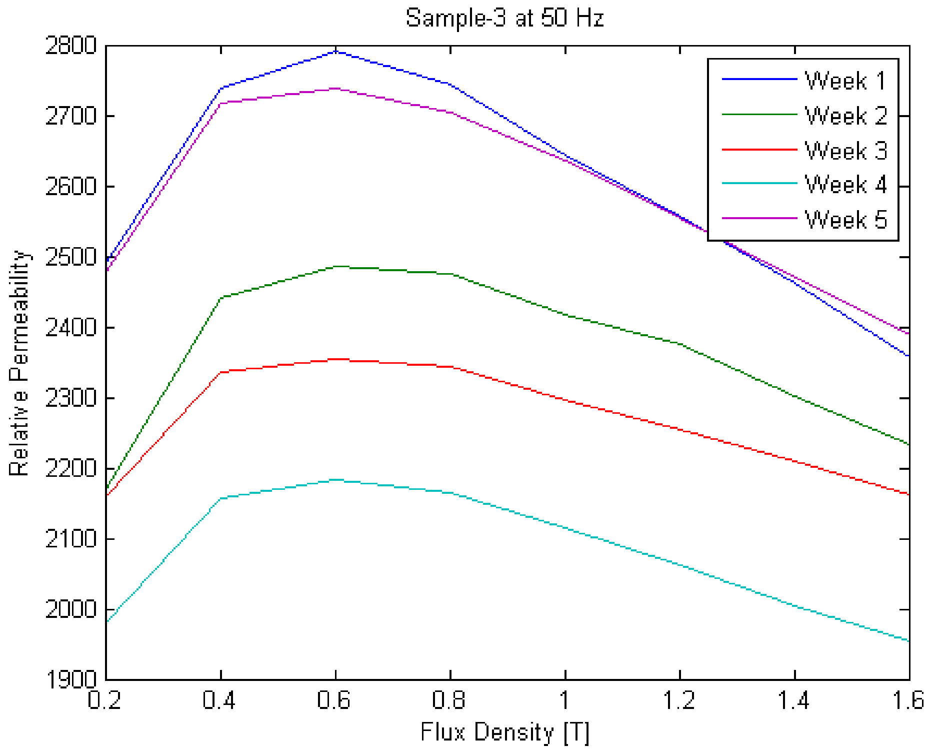

Figure 5.7. Change in relative permeability of Sample 3 at 50 Hz

5.5 ANSYS Simulation to study the effects of decrease in relative permeability

In order to study the effects of decrease in permeability on the inductance and therefore the machine performance, Finite element analysis (FEA) was performed. It investigated the impact of change in relative permeability of ferromagnetic core on the overall properties of the machine. IPMSM machine was used for the simulation.

5.5.1 Theory

The electromagnetic torque of an IPMSM motor is calculated by the following equation [38], [39]:

$$T_e = 3(\frac{N_P}{2})(\lambda_{PM} I_q - (L_q - L_d) I_q I_d) \tag{5.1}$$

$$L_d = L_l + \frac{3}{2}(L_0 + L_2) \tag{5.2}$$

$$L_q = L_l + \frac{3}{2}(L_0 - L_2) \tag{5.3}$$

The self-inductance of the machine is given by the following equation [23]:

$$L = L_0 + L_l + L_2 cos2\theta \tag{5.4}$$

L_0 is the inductance due to space fundamental air-gap flux, L_l is the leakage flux component L_2 is the second harmonic component and θ is the rotor electrical angle. N_p and λ_{PM} are the number of poles and flux linkage, respectively. L_q, L_d, I_q and I_d are the d and q total inductances, and current respectively.

FEA analysis of an IPMSM machine model was conducted to observe the effects of decrease in permeability on the rotor performance. It was observed that, with the decrease in permeability of the rotor core, L_d and L_q decreased due to the increase in reluctance of the rotor steel leg which was in contact with the magnet.

5.5.2 ANSYS Simulation

A transient simulation analysis was conducted on an IPMSM model made available by Ansys. Figure 5.8 shows the model used to study the change in inductances with decrease in relative permeability [44].

The 360 W, 4 pole pair machine with an exterior diameter of 290 mm, rotating at a speed of 1500 rpm was used for the simulation. The stator had 24 slots and was divided into three phases, powered by 220 V rated voltage.The air-gap between the stator and rotor was fixed at 1.5mm.

The relative permeability values were taken from the experimental results for Sample 3 laminations at 50 Hz and 0.6 T, over a four week period.

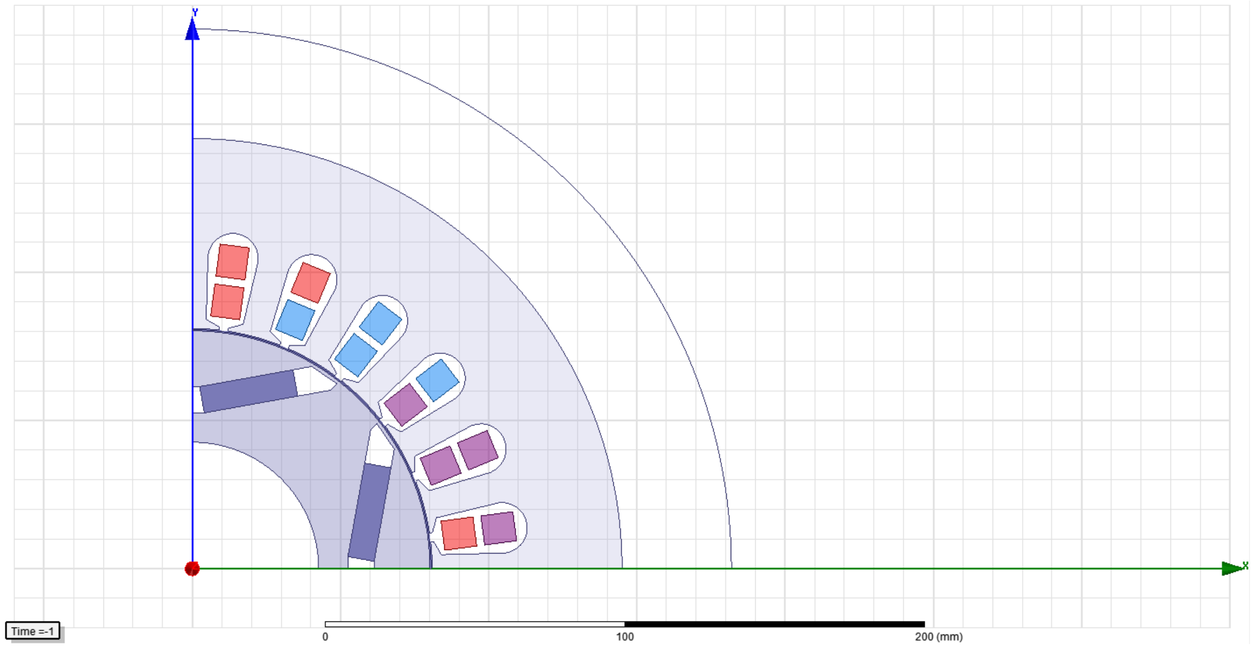

Figure 5.8. IPMSM Machine Model in Maxwell Ansys

The stator and shaft was maintained at week-1 permeability value, whereas the rotor permeability was changed for each simulation. The L_d and L_q values were calculated from the simulation by running a parametric analysis.

Figure 5.9 shows the decrease in inductance along the d-axis of the IPMSM motor.

It was observed from the graph that the inductance along the d-axis decreased by approximately 2% by the end of the fourth week.

Figure 5.10 shows the decrease in inductance along the q-axis of the IPMSM motor.

The inductance along the q-axis was also found to decrease by the end of the fourth week. It can be observed from Figure 5.9 and Figure 5.10 that the decrease in inductance along the d-axis was much higher in comparison to the decrease in inductance along the q-axis.

Figure 5.11 shows the change in rotor torque at a fixed operating condition. The speed of the IPMSM machine was fixed at 1500 rpm and the maximum current of -30A was given as the input. The rotor angle was fixed at 52.5 degrees.

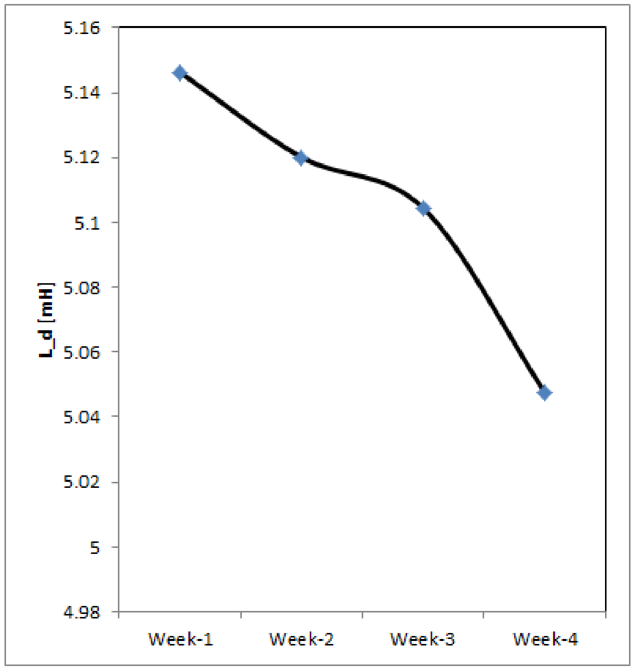

Figure 5.9. Decrease in Inductance along d-axis

It was observed that the rotor torque was highest for week-4 and was minimum for week-1. It could thus be concluded that high-energy magnets do have effects on the machine and it varies with change in operating conditions.

It was also observed that (L_q-L_d) increased with the decrease in relative permeability of the rotor core. From 5.11, it can be calculated that increase in (L_q-L_d) would lead to a decrease in the electromagnetic torque thus having an effect on the machine. As previously mentioned, this effect is different depending on the operating conditions of speed and torque.

The simulations were conducted with a fixed air-gap of 1.5mm. According to [49], change in the air-gap length in case of an IPMSM machine was found to affect the inductance along the q-axis significantly while it did not have much effect on the d-axis.

Therefore, it can be concluded that for machines with air-gap lesser than 1.5mm, the influence of high-energy magnets would be much more significant thus affecting the performance of the machine.

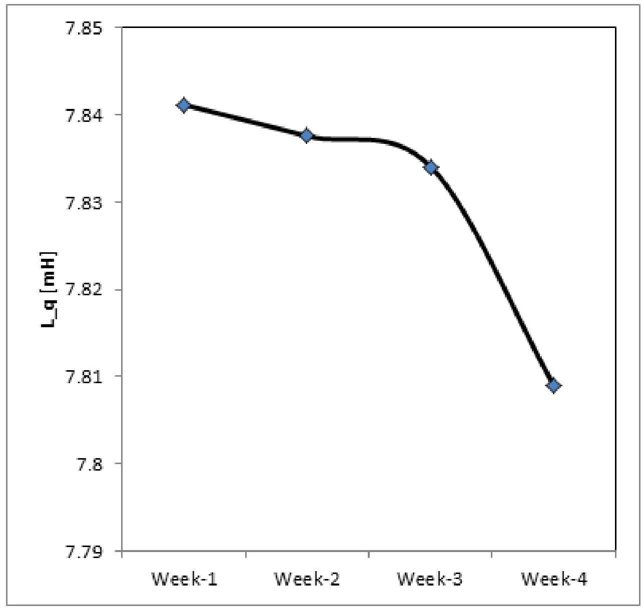

Figure 5.10. Decrease in Inductance along q-axis

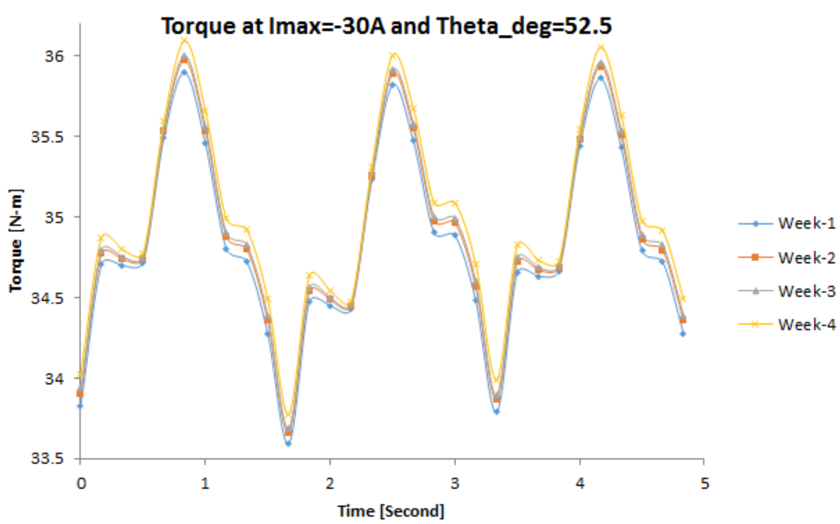

Figure 5.11. Comparison of Rotor Torque at -30A

5.6 Conclusion

Three samples of M-19 gage 29 non-oriented magnetic steel were studied using a B-H analyzer to find the effects of high-energy Neodymium permanent magnets on the magnetic properties of the samples.

The samples were tested under different conditions and it was concluded that the presence of high energy magnets reduced the relative permeability of the ferromagnetic core. The relative permeability of the magnets was regained under two conditions, when the polarity of the magnets was changed, and when the cores were no longer exposed to the high energy magnets.

It could therefore be concluded that it is very important to consider this factor while designing the core of PM motors since the decrease in relative permeability leads to increase in reluctance of the magnetic circuit which in turn affects the inductance and flux density, hence compromising the performance of the machine.

Future work in this area of study can be focused on selecting closed cores for the experiment in order to calculate the exact decrease in permeability and to increase the precision of the experiment. Further experiments can be conducted by placing the magnets in different positions of the steel core and noting down its effects on the performance of the machine.

CHAPTER 6

THESIS CONCLUSION

In this research, two critical factors were considered that affected the performance of a machine. The first factor was the effect of manufacturing techniques on the magnetic properties of the lamination that changed the relative permeability and core loss of the core and the second factor was the influence of high-energy magnets on the magnetic properties of the rotor laminations in IPMSM and SPMSM machines.

This research also studied the effects of change in B-H curves on a machine performance by comparing the magnetizing currents under linear, saturation and non-linear hysteresis conditions.

In order to study the effects of cutting techniques on the relative permeability and core loss of a machine, experiments were conducted using samples of different cutting techniques and results were obtained using a B-H analyzer. The surface finish of each cut was examined using a digital microscope and the relevance of the same was proved with respect to the air-gap between the rotor and the stator cores.

Comparisons were made between the different cutting techniques and conclusion was drawn that the water-jet cutting technique had the least detrimental effects on the performance of the machine.

Experiments were also conducted to note the influence of post annealing process on the magnetic properties of steel laminations. It was concluded that the post-annealing process improved the relative permeability and decreased the core loss of the machine.

With reference to the second factor related to the high-energy magnets, experiments were conducted for a prolonged period of five weeks. The samples were tested under various conditions. It was concluded that in every condition, the relative permeability of the sample decreased when it was kept in continuous contact with high-energy magnets.

The magnetic properties of the core were regained under two conditions. The first was when the polarity of the magnets were changed and kept in opposite direction in comparison to the first case and the second was when the magnets were removed and the core was kept in isolation.

The torque and inductance characteristics were studied and it was concluded that this decrease in the relative permeability had different effects under different operating conditions.

The d-axis and q-axis inductances were found to decrease when the core was kept in contact with the high-energy magnets. But under certain conditions of maximum current of -30A and torque angle of 52.5 degrees, the rotor torque increased when the core was kept in prolonged contact with the high-energy magnets.

Thus it is concluded that it is important to study these effects and take it into consideration while designing motors as it may have effects on the performance of the machines.

REFERENCES

[1] Coercivity. https://en.wikipedia.org/wiki/Coercivity/. Accessed: 2016-12-22.

[2] Five factors that mess up motor efficiency and how to improve it. http://electrical-engineering-portal.com/5-factors-that-mess-up-motor-efficiency-and-how-to-improve-it. Accessed: 2016-12-19.

[3] Keyence digital microscope.

[4] Neodymium iron boron magnets. http://www.electronenergy.com/products/materials/neodymium-iron-boron/. Accessed: 2016-12-19.

[5] Samarium cobalt magnets. http://www.electronenergy.com/products/materials/samarium-cobalt/. Accessed: 2016-12-19.

[6] Alessandro, B., C. Beatrice, G. Bertotti, and A. Montorsi (1990). Domain-wall dynamics and barkhausen effect in metallic ferromagnetic materials. i. theory. *Journal of applied physics 68*(6), 2901–2907.

[7] Ali, K., K. Atallah, and D. Howe (1997). Prediction of mechanical stress effects on the iron loss in electrical machines. *Journal of applied physics 81*(8), 4119–4121.

[8] Bertotti, G. (1984). Space-time correlation properties of the magnetization process and eddy current losses: Applications. i. fine wall spacing. *Journal of applied physics 55*(12), 4339–4347.

[9] Bertotti, G. (1985). Physical interpretation of eddy current losses in ferromagnetic materials. i. theoretical considerations. *Journal of applied Physics 57*(6), 2110–2117.

[10] Boglietti, A., A. Cavagnino, M. Lazzari, and M. Pastorelli (2001). Effects of punch process on the magnetic and energetic properties of soft magnetic material. In *Electric Machines and Drives Conference, 2001. IEMDC 2001. IEEE International*, pp. 396–399. IEEE.

[11] Bozorth, R. (1935). Electrical engineering. pp. 1251.

[12] Brailsford, F., D. A. Oliver, D. Hadfield, and G. R. Polgreen (1948, December). Magnetic materials. a review of progress. *Electrical Engineers - Part I: General, Journal of the Institution of 95*(96), 522–543.

[13] Broddefalk, A. and M. Lindenmo (2006). Dependence of the power losses of a non-oriented 3% si-steel on frequency and gauge. *Journal of Magnetism and Magnetic Materials 304*(2), e586–e588.

[14] Chen, Y. and P. Pillay (2002). An improved formula for lamination core loss calculations in machines operating with high frequency and high flux density excitation. In *Industry Applications Conference, 2002. 37th IAS Annual Meeting. Conference Record of the*, Volume 2, pp. 759–766. IEEE.

[15] Chikazumi, S. and C. D. Graham (2009). *Physics of Ferromagnetism 2e*. Number 94. Oxford University Press on Demand.

[16] Cullity, B. D. and C. D. Graham (2009a). *Definitions and Units*, pp. 1–21. Wiley-IEEE Press.

[17] Cullity, B. D. and C. D. Graham (2009b). *Domains and the Magnetization Process*, pp. 275–333. Wiley-IEEE Press.

[18] Cullity, B. D. and C. D. Graham (2009c). *Experimental Methods*, pp. 23–86. Wiley-IEEE Press.

[19] Cullity, B. D. and C. D. Graham (2009d). *Ferromagnetism*, pp. 115–149. Wiley-IEEE Press.

[20] Cullity, B. D. and C. D. Graham (2009e). *Hard Magnetic Materials*, pp. 477–504. Wiley-IEEE Press.

[21] Deane, J. H. (1994). Modeling the dynamics of nonlinear inductor circuits. *IEEE Transactions on Magnetics 30*(5), 2795–2801.

[22] Emura, M., F. Landgraf, W. Ross, and J. Barreta (2003). The influence of cutting technique on the magnetic properties of electrical steels. *Journal of Magnetism and Magnetic Materials 254*, 358–360.

[23] Fitzgerald, A. E., C. Kingsley, S. D. Umans, and B. James (2003). *Electric machinery*, Volume 5. McGraw-Hill New York.

[24] Fourness, C. A. e. a. (1935). Paper metering, cutting, and reeling.

[25] Hilton, P. A. (2007). The early days of laser cutting. *11th Nordic Conference in Laser Processing of Materials, Lappeenranta, Finland*.

[26] Ionel, D. M., M. Popescu, S. J. Dellinger, T. Miller, R. J. Heideman, and M. I. McGilp (2006). On the variation with flux and frequency of the core loss coefficients in electrical machines. *IEEE Transactions on Industry Applications 42*(3), 658–667.

[27] Jiles, D. and D. Atherton (1986). Theory of ferromagnetic hysteresis. *Journal of magnetism and magnetic materials 61*(1-2), 48–60.

[28] Joule, J. (1847). Philosophical magazine. pp. 76–225.

[29] Kis, P. and A. Iványi (2004). Parameter identification of jiles–atherton model with nonlinear least-square method. *Physica B: Condensed Matter 343*(1), 59–64.

[30] Krings, A. (2014). Iron losses in electrical machines-influence of material properties, manufacturing processes, and inverter operation.

[31] Krings, A. and J. Soulard (2010). Overview and comparison of iron loss models for electrical machines. In *5th International Conference and Exhibition on Ecological Vehicles and Renewable Energies (EVER 10), Monte-Carlo, MONACO, MAR 25-28, 2010*.

[32] L. Gu, S. Jayasankar, D. H. E. B. M. W. and B. Fahimi (2016). Evaluation of the influence of different cutting methods on permeability and core losses in magnetic steel. In *17th Biennial Conference on Electromagnetic Field Computation*. IEEE.

[33] Lascoe, O. D. (1966). 6b: Design considerations for stamping. *Handbook of Fabrication Processes*, 435.

[34] Lazari, P., K. Atallah, and J. Wang (2015). Effect of laser cut on the performance of permanent magnet assisted synchronous reluctance machines. *IEEE Transactions on Magnetics 51*(11), 1–4.

[35] Loisos, G. and A. J. Moses (2005). Effect of mechanical and nd: Yag laser cutting on magnetic flux distribution near the cut edge of non-oriented steels. *Journal of materials processing technology 161*(1), 151–155.

[36] Martindale, R. G. (1948, October). Anisotropic strains produced by surface abrasion, and their effect on the magnetic properties of silicon sheet steel. *Electrical Engineers - Part II: Power Engineering, Journal of the Institution of 95*(47), 620–626.

[37] MATLAB (2010). *version 7.10.0 (R2010a)*. Natick, Massachusetts: The MathWorks Inc.

[38] Miller, T. (1989). *Permanent Magnet and Reluctance Motor Drives*. Oxford, UK: Oxford Science Publications.

[39] Mirahki, H. and M. Moallem (2014). Torque calculation in interior permanent magnet synchronous machine using improved lumped parameter models. *Progress In Electromagnetics Research M 39*, 131–139.

[40] Moses, A., N. Derebasi, G. Loisos, and A. Schoppa (2000). Aspects of the cut-edge effect stress on the power loss and flux density distribution in electrical steel sheets. *Journal of Magnetism and Magnetic Materials 215*, 690–692.

[41] Pitman, K. C. (1990, Sep). The influence of stress on ferromagnetic hysteresis. *IEEE Transactions on Magnetics 26*(5), 1978–1980.

[42] Reinlein, M., T. Hubert, A. Hoffmann, and A. Kremser (2013). Optimization of analytical iron loss approaches for electrical machines. In *Electric Drives Production Conference (EDPC), 2013 3rd International*, pp. 1–7. IEEE.

[43] Rygal, R., A. Moses, N. Derebasi, J. Schneider, and A. Schoppa (2000). Influence of cutting stress on magnetic field and flux density distribution in non-oriented electrical steels. *Journal of magnetism and Magnetic Materials 215*, 687–689.

[44] S. Jayasankar, L. Maharjan, E. C. E. B. and B. Fahimi (2017). On the proximity effects of high-energy magnets on m-19 magnetic steel core. In *International Electric Machines and Drives Conference*. IEEE.

[45] Schoppa, A., J. Schneider, and J.-O. Roth (2000). Influence of the cutting process on the magnetic properties of non-oriented electrical steels. *Journal of magnetism and magnetic materials 215*, 100–102.

[46] Serpico, C., C. Visone, I. Mayergoyz, V. Basso, and G. Miano (2000). Eddy current losses in ferromagnetic laminations. *Journal of Applied Physics 87*(9), 6923–6925.

[47] Siebert, R., J. Schneider, and E. Beyer (2014). Laser cutting and mechanical cutting of electrical steels and its effect on the magnetic properties. *IEEE Transactions on Magnetics 50*(4), 1–4.

[48] Spaldin, N. A. (2011). Magnetic materials-fundamentals and applications. 2ª edição.

[49] Sriram, N. (1997). Design optimization of an interior permanent magnet motor.

[50] Steinmetz, C. P. (1892). On the law of hysteresis. *Transactions of the American Institute of Electrical Engineers 9*(1), 1–64.

[51] Ulintz, P. (Oct. 2011). Hole extrusions–part 1. *Metalforming Magazine*.

[52] Yensen, T. D. (1924, Jan). The magnetic properties of the ternary alloys fe-si-c. *Transactions of the American Institute of Electrical Engineers XLIII*, 145–175.

[53] Zhang, Y., M.-C. Cheng, P. Pillay, and B. Helenbrook (2009). High order finite element model for core loss assessment in a hysteresis magnetic lamination. *Journal of Applied Physics 106*(4), 043911.

BIOGRAPHICAL SKETCH

Seethal Jayasankar was born on April 4, 1991 in Tamil Nadu, India. She received her B.E degree in Electrical and Electronics Engineering from Birla Institute of Technology, Mesra, India in 2012. From 2012 to 2015, she worked with GMR Delhi International Airport Ltd. (DIAL), New Delhi, India as an Electrical Engineer. Her work was mainly focused on designing, testing and commissioning of substation and electrical equipment for the construction of India's tallest Air traffic control tower (ATC). She joined the Renewable Energy and Vehicular Technology (REVT) laboratory at The University of Texas at Dallas (UTD) in Summer 2016 as a Graduate Researcher. She has submitted this thesis as a Master of Science student of Power Electronics and Energy system. Her research interests include power electronics, motor drives and renewable energy systems.

CURRICULUM VITAE

Seethal Jayasankar

June 13, 2017

Contact Information:

Department of Electrical Engineering
The University of Texas at Dallas
800 W. Campbell Rd.
Richardson, TX 75080-3021, U.S.A.

Voice: (972) 883-6755
Fax: (972) 883-2710
Email: sxj150730@utdallas.edu

Educational History:

B.E., Electrical and Electronics Engineering, Birla Institute of Technology, 2012

Employment History:

Associate Consultant Intern, Intertek, October 2016 – present
Student Worker, The University of Texas at Dallas, January 2016 – April 2016
Electrical Engineer, GMR Group Delhi International Airport Ltd., July 2012 – May 2015

Professional Recognitions and Honors:

UTD Indian Alumni scholarship, The University of Texas at Dallas, 2015
Employee of the Month, Delhi International Airport, 2013

Professional Memberships:

Institute of Electrical and Electronics Engineers (IEEE), 2016–present